Space-time domain decomposition for two-phase flow between different rock types

Elyes Ahmed, Caroline Japhet, Michel Kern

SPACE-TIME DOMAIN DECOMPOSITION FOR TWO-PHASE FLOW BETWEEN DIFFERENT ROCK TYPES*

ELYES AHMED†, CAROLINE JAPHET‡, AND MICHEL KERN§

Abstract. In [1] a space–time domain decomposition method was proposed for two-phase flow in a porous medium composed of two different rock types, so that the capillary pressure field is discontinuous at the interface between the rocks. For this nonlinear and degenerate parabolic problem, with nonlinear and discontinuous transmission conditions on the interface, the Optimized Schwarz waveform relaxation method (OSWR) with Robin or Ventcell transmission conditions is considered. A guaranteed and fully computable a posteriori error estimate was derived, which in particular took into account the domain decomposition error.

In this paper we provide a mathematical and numerical analysis of this space–time domain decomposition method in the Robin case. Complete numerical approximation is achieved by a finite volume scheme in space and the lowest order discontinuous Galerkin method in time. We prove the existence of a weak solution of the two-phase flow subdomain problem with Robin boundary conditions by analyzing the convergence of the finite volume scheme. The domain decomposition algorithm is based on the solution of space-time nonlinear subdomain problems over the whole time interval, allowing for different time steps in different parts of the domain, adapted to the physical properties of each subdomain, and we show that such an algorithm is well-defined. Numerical experiments on three-dimensional problems with different rock types illustrate the performance of the domain decomposition method.

Key words. Two-phase Darcy flow, discontinuous capillary pressure, finite volume scheme, space–time domain decomposition method, optimized Schwarz waveform relaxation, nonlinear and discontinuous Robin transmission conditions, nonconforming time grids.

1. Introduction.

Simulations of two-phase flows through heterogeneous porous media are widely used in many applications. Among others, these models are used for gas migration around a nuclear waste repository in the subsurface, CO2 sequestration in saline aquifers, or in petroleum engineering to predict the motion of oil in the underground. In such applications, the domain of calculation is a union of different rock types with different physical properties and in which the lengths of the rocks and the time scales may be highly different. Variation of the rock type means variation on the permeability but also on the relative permeability and on the capillary pressure curves, that are functions of the phase saturations. An important consequence, which is the main topic of this paper, is that the capillary pressure and the relative permeability functions may be discontinuous across the interface between different rocks. These discontinuities play a crucial role in many phenomenas see e.g. [7, 9, 19, 18, 57]. The numerical simulation of such flows is a challenging task, and one might want to use much larger time steps for some region of the domain than for others.

In this paper a simplified two-phase flow model is considered (with one equation and no advection), see [31], to study the phenomenon of oil or gas trapping in a porous medium with several rock types. This problem presents several theoretical and numerical difficulties : the *nonlinearity* and *degeneracy* of the parabolic equation for the saturation of one of the phases, and the *nonlinear* and *discontinuous transmission conditions* at the interface between the rocks. First analytical results have been provided by [8, 18, 57], and several numerical schemes have been introduced in [31, 32]

*This work was funded by the French ANR DEDALES under grant ANR-14-CE23-0005.

†Centre de recherche Inria de Paris, 2 rue Simone Iff, 75012 Paris, France, elyes.ahmed@inria.fr

‡Université Paris 13, Sorbonne Paris Cité, LAGA, CNRS (UMR 7539), 93430, Villetaneuse, France, japhet@math.univ-paris13.fr

§Centre de recherche Inria de Paris, 2 rue Simone Iff, 75012 Paris, France, michel.kern@inria.fr

and studied in [20, 22, 31]. More precisely, existence of a weak solution has been proven in [31] using the convergence of a finite volume scheme (see also [22, 23, 20] for the full two-phase flow model). Uniqueness of a weak solution for this model is proved in [22] for a particular choice of functions characterizing the porous medium, and in [25, 23] in the one-dimensional case, for the full two-phase problem with advection terms. In [20], the convergence of the numerical approximation of the full problem in a heterogeneous multidimensional porous medium is proved, without any simplification on the model or particular assumption. Others related works can be found for instance in [24, 34, 52]. Due to different hydrogeological properties of the different rocks, domain decomposition (DD) methods appear to be a natural way to solve efficiently two-phase flow models, see [59, 60], and also [40, 55, 56].

In the companion paper [1] we proposed a *global-in-time* domain decomposition method for this nonlinear and degenerate parabolic problem, that uses the Optimized Schwarz waveform relaxation algorithm (OSWR) with Robin or Ventcell transmission conditions. A guaranteed and fully computable a posteriori error estimate was derived for the finite volume – backward Euler approximation of the proposed space-time DD algorithm, which in particular took into account the domain decomposition error and the linearization error. This enabled the design of a stopping criterion for the OSWR algorithm as well as for the linearization iterations, which together lead to important computational savings. This DD method also allows for simultaneously: a) degenerate parabolic problems; b) nonlinear and discontinuous transmission conditions; c) Robin and Ventcell transmission conditions; d) global-in-time formulation, ans we are not aware of any domain decomposition algorithm proposed and analyzed in that case. Some of these ingredients have been introduced previously independently in [15, 46, 16, 41, 43, 54] and the references therein. The use of optimized (Robin or Ventcell) transmission operators allows physically more valuable information to be exchanged between the subdomains and improves drastically convergence rates, see [49, 51, 15, 35, 46, 48] and the references therein for linear problems, and [21, 41] for problems with nonlinear reaction terms. The use of a global-in-time DD method together with discontinuous Galerkin (DG) for the time discretization provides flexibility in using different time steps in different parts of the domain, adapted to the physical properties of each subdomain, see [45, 46, 47] for diffusion and advection-diffusion problems.

The purpose of this paper is to prove the *existence of a weak solution* to the two-phase flow subdomain problem with Robin boundary conditions, by analyzing the convergence of the finite volume scheme, extending the work in [31]. This in turn will enable us to prove that the space–time domain decomposition algorithm, based on solving space-time nonlinear Robin subdomain problems over the whole time interval, with the possibility of different time stepping in different parts of the domain, is well-defined.

In Section 2 we recall the physical model and define a multidomain weak solution. Then, in Section 3, we recall, in the Robin case, the space-time DD method introduced in [1] , and give the associated interface problem. In Section 4, after introducing the discrete Robin problem in a subdomain based on a finite volume scheme and the lowest order DG method for the time discretization, we prove the existence of a weak solution of the two-phase flow subdomain problem with Robin boundary conditions, by analyzing the convergence of the finite volume scheme. Then, in Section 5 we show that our discrete space-time DD algorithm is well-defined. The method is numerically validated on several examples in three space dimensions in Section 6.

2. Presentation of the problem. Most of the content of this section, with the important exception of the definition of a weak solution, is taken from the companion paper [1], which is complementary to the present work by presenting error estimates and stopping criteria for the domain decomposition iterations. Most of this material actually goes back to [31], and has been included in order to keep the present paper self–contained.

Let Ω be an open bounded domain of $\mathbb{R}^d$, $d = 2$ or 3, which is assumed to be polygonal if $d = 2$ and polyhedral if $d = 3$. We denote by $\partial\Omega$ its boundary (supposed to be Lipschitz-continuous) and by $\mathbf{n}$ the unit normal to $\partial\Omega$, outward to Ω. Let a time interval $(0, T)$ be given with $T > 0$. We consider a simplified model of a two-phase flow through a heterogeneous porous medium, in which the advection is neglected. Assuming that there are only two phases occupying the porous medium Ω, say gas and water, and that each phase is composed of a single component, the mathematical form of this problem as it is presented in [22, 31] is as follows: given initial and boundary gas saturations u_0 and g, as well as a source term f, find $u : \Omega \times [0, T] \to [0, 1]$ such that

$$\partial_t u - \nabla \cdot (\lambda(u, \mathbf{x})\nabla\pi(u, \mathbf{x})) = f, \quad \text{in } \Omega \times (0, T), \tag{2.1a}$$

$$u(\cdot, 0) = u_0, \quad \text{in } \Omega, \tag{2.1b}$$

$$u = g, \quad \text{on } \partial\Omega \times (0, T). \tag{2.1c}$$

Here u is the *gas saturation* (and therefore $(1 - u)$ is the water saturation), $\pi(u, \mathbf{x}) : [0, 1] \times \Omega \to \mathbb{R}$ is the *capillary pressure*, and $\lambda(u, \mathbf{x}) : [0, 1] \times \Omega \to \mathbb{R}$ is the *global mobility* of the gas given by

$$\lambda(u) = \frac{\lambda_{\mathrm{w}}(1 - u)\lambda_{\mathrm{g}}(u)}{\lambda_{\mathrm{w}}(1 - u) + \lambda_{\mathrm{g}}(u)},$$

where λ_{w} and λ_{g} are the phase mobilities. One can refer to [26, 27, 31] for a derivation of (2.1) from the complete two-phase flow model.

For simplicity, we consider only Dirichlet boundary conditions on $\partial\Omega$. Other types of boundary conditions could be dealt with the same way as in [22, 31, 58]. The model problem given by (2.1a) is a nonlinear degenerate parabolic problem as the global mobility $\lambda(u) \to 0$ for $u \to 0$ and 1, and, moreover, $\pi'(u) \to 0$ for $u \to 0$ (see [14, 27]).

2.1. Flow between two rock types. In this part, we particularize the model problem (2.1a) to a porous medium with different capillary pressure curves π_i in each subdomain, following [31]. For simplicity we suppose that Ω is composed of two non-overlapping subdomains Ω_i, $i = 1, 2$, which are both open polygonal subsets of $\mathbb{R}^d$ with Lipschitz-continuous boundary. However, the analysis given below can be generalized to the case of multiple subdomains (see Section 6).

We denote by Γ the interface between Ω_1 and Ω_2, i.e., $\Gamma = (\partial\Omega_1 \cap \partial\Omega_2)^\circ$. Let $\Gamma_i^{\mathrm{D}} = \partial\Omega_i \cap \partial\Omega$. Both data λ and π, which can in general depend on the physical characteristics of the rock, are henceforth supposed to be homogeneous in each subdomain Ω_i, $i = 1, 2$, i.e., $\lambda_i(\cdot) := \lambda_{|\Omega_i}(\cdot) = \lambda(\cdot, \mathbf{x}), \forall \mathbf{x} \in \Omega_i$, and similarly for π_i. The equations (2.1a) in *each subdomain* Ω_i then read as

$$\partial_t u_i - \nabla \cdot (\lambda_i(u_i)\nabla\pi_i(u_i)) = f_i, \quad \text{in } \Omega_i \times (0, T), \tag{2.2a}$$

$$u_i(\cdot, 0) = u_0, \quad \text{in } \Omega_i, \tag{2.2b}$$

$$u_i = g_i, \quad \text{on } \Gamma_i^{\mathrm{D}} \times (0, T). \tag{2.2c}$$

We use the notation $v_i = v|_{\Omega_i}$ for an arbitrary function v.

Before transcribing the transmission conditions on the interface Γ, we make precise the assumptions on the data (further generalizations are possible, bringing more technicalities):

ASSUMPTION 2.1 (Data).

1. *For $i \in \{1,2\}$, $\pi_i \in C^1([0,1],\mathbb{R})$ can be extended in a continuous way to a function (still denoted by π_i) such that $\pi_i(u) = \pi_i(0)$ for all $u \leq 0$ and $\pi_i(u) = \pi_i(1)$ for all $u \geq 1$. Moreover, $\pi_i|_{[0,1]}$ is a strictly increasing function. Following [31], we also assume that $\pi_1(0) \leq \pi_2(0) < \pi_1(1) \leq \pi_2(1)$.*
2. *For $i \in \{1,2\}$, $\lambda_i \in C^0([0,1],\mathbb{R}^+)$ is bounded and can be extended in a continuous way to a function (still denoted by λ_i) such that $\lambda_i(u) = \lambda_i(0)$ for all $u \leq 0$ and $\lambda_i(u) = \lambda_i(1)$ for all $u \geq 1$. We denote by C_λ an upper bound of $\lambda_i(u)$, $u \in \mathbb{R}$.*
3. *The initial condition is such that $u_0 \in L^\infty(\Omega)$ with $0 \leq u_0 \leq 1$ a.e. in Ω.*
4. *The boundary conditions $0 \leq g_i \leq 1$ are traces of some functions from $L^2(0,T;H^1(\Omega_i))$. Moreover, they need to match in the sense that $\pi_1(g_1(\mathbf{x})) = \pi_2(g_2(\mathbf{x}))$ for all $\mathbf{x} \in \Gamma \cap \Gamma_1^{\mathrm{D}}$ and all $\mathbf{x} \in \Gamma \cap \Gamma_2^{\mathrm{D}}$.*
5. *The source term is such that $f \in L^2(0,T;L^2(\Omega))$. For simplicity we further assume that f is piecewise constant in time with respect to the temporal mesh introduced in subsection 4.1.2 below.*

We give now the *transmission conditions* needed to connect the subdomain problems (2.2), for $i = 1, 2$. We consider two cases. The first case is when

$$\pi_1(0) = \pi_2(0) \qquad \text{and} \qquad \pi_1(1) = \pi_2(1), \tag{2.3}$$

the same way as in [22]. If the functions π_i satisfy the above condition, the capillarity curves are said to be matching and the resulting transmission conditions on the interface are given by

$$\pi_1(u_1) = \pi_2(u_2), \qquad \text{on } \Gamma \times (0,T), \tag{2.4a}$$

$$\lambda_1(u_1)\nabla\pi_1(u_1)\cdot\mathbf{n}_1 = -\lambda_2(u_2)\nabla\pi_2(u_2)\cdot\mathbf{n}_2, \quad \text{on } \Gamma \times (0,T). \tag{2.4b}$$

These conditions yield a discontinuous saturation across the interface, i.e., we find that in general $u_1 \neq u_2$ on Γ.

In the second case, i.e., in the case when

$$\pi_1(0) \neq \pi_2(0) \qquad \text{or} \qquad \pi_1(1) \neq \pi_2(1), \tag{2.5}$$

the capillarity pressure curves are said to be non-matching. Consequently, not only the saturation is discontinuous at the medium interface, but also the capillary pressure field. The condition (2.5), studied in [31], has direct consequences on the behavior of the capillary pressures on both sides of the interface Γ. Indeed, because of Assumption 2.1–1, there exists two unique real numbers $(u_1^*, u_2^*) \in [0,1]^2$ satisfying respectively $\pi_1(u_1^*) = \pi_2(0)$ and $\pi_2(u_2^*) = \pi_1(1)$. Then, if $u_1 \geq u_1^*$ and $u_2 \leq u_2^*$, we can still prescribe the connection of the capillary pressures $\pi_1(u_1) = \pi_2(u_2)$ on the interface Γ as in (2.4a). If $0 \leq u_1 \leq u_1^*$, the model imposes $u_2 = 0$, and the gas phase is entrapped in the rock Ω_1, and the water flows across Γ. In the same way, if $u_2^* \leq u_2 \leq 1$, the model prescribes $u_1 = 1$, and the water phase is captured in Ω_2 as a discontinuous phase, and the gas flows across Γ (see Fig. 2.1 left). Following [27, 31],

these conditions on the gas-water saturations on the interface Γ are simply given by

$$\overline{\pi}_1(u_1) = \overline{\pi}_2(u_2), \qquad \text{on } \Gamma \times (0,T), \tag{2.6a}$$

$$\lambda_1(u_1)\nabla\pi_1(u_1)\cdot\mathbf{n}_1 = -\lambda_2(u_2)\nabla\pi_2(u_2)\cdot\mathbf{n}_2, \quad \text{on } \Gamma \times (0,T), \tag{2.6b}$$

where $\overline{\pi}_i$, for $i = 1, 2$, are truncated capillary pressure functions given on $[0,1]$ respectively by $\overline{\pi}_1 : u \mapsto \max(\pi_1(u), \pi_2(0))$ and $\overline{\pi}_2 : u \mapsto \min(\pi_2(u), \pi_1(1))$ (see Fig. 2.1 right). In [31], it has been established that the model problem (2.2) together with the transmission conditions (2.6) has the necessary mathematical properties to explain the phenomena of gas trapping (see also [11, 25]).

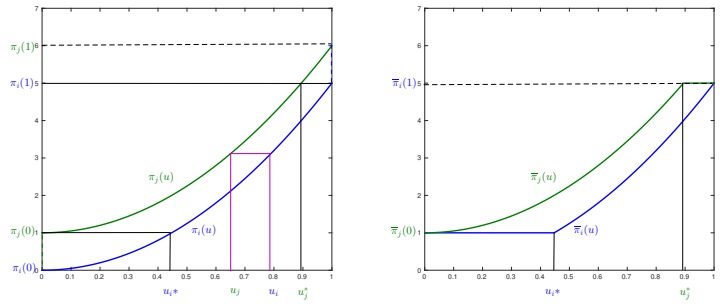

FIG. 2.1. *Capillary pressure curves (left) and truncated capillary pressures curves (right)*

2.2. Transformation of the equations and weak formulation. Still following [31], we present here the mathematical quantities and function spaces used to characterize the weak solution to the multidomain problem (2.2) with the conditions (2.6). That of the problem (2.2) with the conditions (2.4) can be deduced straightforwardly from this later, see [22]. As Ω_i is a homogeneous rock type, so that π_i and λ_i do not depend on $\mathbf{x}$, one can define the Kirchhoff transform

$$\varphi_i : \left\{ \begin{array}{ccc} [0,1] & \longrightarrow & \mathbb{R}^+ \\ s & \longmapsto & \int_0^s \lambda_i(a)\pi_i'(a)\mathrm{d}a. \end{array} \right. \tag{2.7}$$

The function φ_i is Lipschitz-continuous and increasing on $[0,1]$, we denote by $L_{\varphi,i}$ its Lipschitz constant and we let $L_\varphi := \max(L_{\varphi,1}, L_{\varphi,2})$. We extend the function φ_i from $[0,1]$ to $\mathbb{R}$ so that $\varphi_i(u) = \varphi_i(0)$ for all $u \le 0$ and $\varphi_i(u) = \varphi_i(1)$ for all $u \ge 1$.

We now introduce the strictly increasing function ϕ by

$$\phi : \left\{ \begin{array}{ccc} [\pi_2(0), \pi_1(1)] & \longrightarrow & \mathbb{R}^+ \\ s & \longmapsto & \displaystyle\int_{\pi_2(0)}^{s} \min_{j\in\{1,2\}} (\lambda_j \circ \pi_j^{-1}(a))\,\mathrm{d}a, \end{array} \right.$$

and let $\Pi_i := \phi \circ \overline{\pi}_i$, for $i \in \{1,2\}$. The functions $\Pi_i|_{[0,1]}$, introduced first in [31, Lemma 1.2] and used in [22, 25], are differentiable and increasing. We let $\Pi_i(u) = \Pi_i(0)$ for all $u \le 0$ and $\Pi_i(u) = \Pi_i(1)$ for all $u \ge 1$ and define the function Π by

$$\Pi(u, \mathbf{x}) = \Pi_i(u), \quad \text{for } \mathbf{x} \in \Omega_i.$$

As Π_i are more regular than $\overline{\pi}_i$, this allows to connect Π_1 and Π_2 instead of $\overline{\pi}_1$ and $\overline{\pi}_2$, that is, for all $(u_1, u_2) \in \mathbb{R}^2$, we have the crucial *equivalence property*

$$\overline{\pi}_1(u_1) = \overline{\pi}_2(u_2) \Leftrightarrow \Pi_1(u_1) = \Pi_2(u_2).$$

Finally, it is shown in [31, Lemma 1.2] that, under Assumption 2.1, the function $\beta_i := \Pi_i \circ \varphi_i^{-1}$ is Lipschitz-continuous with a Lipschitz constant lower than 1:

$$|\Pi_i(a) - \Pi_i(b)| \leq |\varphi_i(a) - \varphi_i(b)|, \quad \forall (a,b) \in [0,1]^2. \tag{2.8}$$

We now apply the Kirchhoff transformation (2.7) separately in each subdomain, giving an equivalent formulation suitable for *mathematical analysis*: find u_i such that

$$\partial_t u_i - \Delta \varphi_i(u_i) = f_i, \qquad \text{in } \Omega_i \times (0,T), \tag{2.9a}$$
$$u_i(\cdot,0) = u_0, \qquad \text{in } \Omega_i, \tag{2.9b}$$
$$\varphi_i(u_i) = \varphi_i(g_i), \quad \text{on } \Gamma_i^{\mathrm{D}} \times (0,T), \tag{2.9c}$$

together with the conditions at the interface relying on the smoother functions Π_i

$$\Pi_1(u_1) = \Pi_2(u_2), \qquad \text{on } \Gamma \times (0,T), \tag{2.10a}$$
$$\nabla \varphi_1(u_1) \cdot \mathbf{n}_1 = -\nabla \varphi_2(u_2) \cdot \mathbf{n}_2, \quad \text{on } \Gamma \times (0,T). \tag{2.10b}$$

Now, we define a weak solution to the multidomain problem (2.9a)–(2.10b). We introduce the notation

$$\begin{aligned} H^1_{\varphi_i(g_i)}(\Omega_i) &:= \{v \in H^1(\Omega_i), v = \varphi_i(g_i) \text{ on } \Gamma_i^{\mathrm{D}}\} \\ H^1_{\Pi(g,\cdot)} &:= \{v \in H^1(\Omega), v = \Pi(g,\cdot) \text{ on } \partial\Omega\}, \\ \tilde{X} &:= \left\{\psi \in H^1(\Omega \times (0,T)),\ \psi = 0 \text{ on } \partial\Omega,\ \psi(.,T) = 0\right\}. \end{aligned}$$

Definition 2.1 (Multidomain weak solution). *A function u is said to be a weak solution to problem (2.9a)–(2.10b) if it satisfies:*

1. $u \in L^\infty(\Omega \times (0,T))$, $0 \leq u(\mathbf{x},t) \leq 1$ *a.e. in* $\Omega \times (0,T)$,
2. $\varphi_i(u_i) \in L^2(0,T; H^1_{\varphi_i(g_i)})$, $i \in \{1,2\}$,
3. $\Pi(u,\cdot) \in L^2(0,T, H^1_{\Pi(g,\cdot)}(\Omega))$,
4. *For all* $\psi \in \tilde{X}$, *the following integral equality holds:*

$$\sum_{i=1}^{2} \int_{\Omega_i} \int_0^T u_i(\mathbf{x},t) \partial_t \psi(\mathbf{x},t)\, d\mathbf{x}dt + \sum_{i=1}^{2} \int_{\Omega_i} u_0(\mathbf{x}) \psi(\mathbf{x},0)\, d\mathbf{x} - \sum_{i=1}^{2} \int_{\Omega_i} \int_0^T \nabla \varphi_i(u_i(\mathbf{x},t)) \cdot \nabla \psi(\mathbf{x},t)\, d\mathbf{x}dt = 0.$$

For a sufficiently regular weak solution u, the continuity of the flux condition, namely $[\nabla \varphi(u) \cdot \mathbf{n}] = 0$ on Γ, is fulfilled by point 4 of the definition while the condition $[\Pi(u)] = 0$ on Γ is imposed in space using point 3. In fact, using point 2 together with the fact that $\Pi \circ \varphi^{-1}$ is a Lipschitz continuous function ensures that $\Pi_i(u_i)$ is in $L^2(0,T,H^1(\Omega_i))$, for $i \in \{1,2\}$, hence the connection of the traces on $\Gamma \times (0,T)$.

Note that the notion of weak solution used in the present paper is different than the one used in [1]. The definition used here is the same as in [31], where the existence of a weak solution in the sense of Definition 2.1 was proved under Assumption 2.1 (for Neumann boundary conditions) using the convergence of a finite volume scheme. A more general notion of weak solution (in particular relaxing the inequalities in Assumption 2.1–1) is introduced in [25], see in particular Remark 2.4 in that paper.

For the case of matching capillary pressure curves, i.e. $\pi_1(0) = \pi_2(0)$ and $\pi_1(1) = \pi_2(1)$, uniqueness is obtained in [22]. For the more general case, uniqueness is obtained in [23, 25] only for the one dimensional case.

3. Space–time domain decomposition method. In this section, we present a non-overlapping space–time domain decomposition to solve the flow problem between rock types (2.9)–(2.10) in parallel. Precisely, an equivalent formulation to the model problem (2.9)–(2.10) can be obtained by solving, for $i = 1, 2$, equations (2.9) together with optimized Robin transmission conditions on $\Gamma \times (0, T)$

$$\begin{aligned} \nabla\varphi_1(u_1)\cdot\mathbf{n}_1 + \alpha_{12}\Pi_1(u_1) &= -\nabla\varphi_2(u_2)\cdot\mathbf{n}_2 + \alpha_{12}\Pi_2(u_2), \\ \nabla\varphi_2(u_2)\cdot\mathbf{n}_2 + \alpha_{21}\Pi_2(u_2) &= -\nabla\varphi_1(u_1)\cdot\mathbf{n}_1 + \alpha_{21}\Pi_1(u_1). \end{aligned} \qquad \text{on } \Gamma\times(0,T), \tag{3.1}$$

where α_{ij} are positive constants that can be optimized to improve the convergence factor of the algorithm, when the resulting multidomain problem is solved iteratively, see Section 3.2. This equivalence of problems (2.9)–(2.10) and (2.9)–(3.1) implies that a weak solution to the latter problem exists, and is unique under the same assumptions (see [22] for more details).

3.1. A Space–Time Interface Problem. An interface operator can be used to reformulate the multidomain problem (2.9)–(3.1) as an equivalent *interface Problem*, where the unknowns are located only on the interface $\Gamma \times (0, T)$, see e.g. [30]. This formulation is based on [46], and one can generalize it as in [5, 6] for the case of multiple subdomains.

We introduce Robin to Robin operators for subdomain Ω_i as follows:

$$\begin{aligned} \mathcal{S}_i : L^2(\Gamma\times(0,T)) &\to L^2(\Gamma\times(0,T)) \\ \xi_i &\to -\xi_i + \alpha_{ij}\pi_i(u_i) + \alpha_{ji}\pi_i(u_i) \end{aligned} \tag{3.2}$$

where u_i is the solution of the subdomain problem with Robin boundary data ξ_i:

$$\begin{aligned} \partial_t u_i - \Delta\varphi_i(u_i) &= 0, && \text{in } \Omega_i\times(0,T), \\ u_i(\cdot,0) &= u_0, && \text{in } \Omega_i, \\ \varphi_i(u_i) &= g_i && \text{on } \Gamma_i^{\mathrm{D}}\times(0,T), \\ \nabla\varphi_i(u_i)\cdot n_i + \alpha_{ij}\pi_i(u_i) &= \xi_i && \text{on } \Gamma\times(0,T). \end{aligned} \tag{3.3}$$

The (non-linear) operator $\mathcal{S}_i$ maps the Robin boundary to the new Robin data that will be transmitted to the neighboring subdomain. Note that, similarly to what was done in [5, Remark 3.1], we have eliminated the normal derivative by making use of the boundary condition, so that the transmitted quantity is actually equal to $-\nabla\varphi_i(u_i)\cdot n_i + \alpha_{ji}\pi(u_i)$. This makes $\mathcal{S}_i$ well defined on $L^2(\Gamma\times(0,T))$. The same technique can be used at the discrete level to avoid computing the normal derivative numerically.

Then, the multidomain problem (2.9)–(3.1) is equivalent to the following interface problem for the two unknowns $(\xi_1, \xi_2) \in L^2(\Gamma\times(0,T))^2$:

$$\begin{aligned} \xi_1 &= \mathcal{S}_2(\xi_2), \\ \xi_2 &= \mathcal{S}_1(\xi_1), \end{aligned} \qquad \text{on } \Gamma\times(0,T). \tag{3.4}$$

This problem is nonlinear and can be solved using Newton or fixed point iterations.

3.2. The Optimized Schwarz Waveform Relaxation Algorithm. A fixed point iteration for solving the nonlinear interface problem (3.4) takes the form

$$\begin{aligned} \xi_1^k &= \mathcal{S}_2(\xi_2^{k-1}), \\ \xi_2^k &= \mathcal{S}_1(\xi_1^{k-1}), \end{aligned} \qquad \text{on } \Gamma \times (0,T). \tag{3.5}$$

This requires the solution, at every iteration $k \geq 1$, of the nonlinear subdomain problem (3.3) in Ω_i, for $i \in \{1,2\}$, to compute the action of the nonlinear operators $\mathcal{S}_1$ and $\mathcal{S}_2$ on ξ_1 and ξ_2, respectively. This fixed-point algorithm is in fact equivalent to the Optimized Schwarz Waveform Relaxation (OSWR) iterative method, introduced in [37, 51] for linear problems, in [21, 41] for problems with nonlinear reaction terms, and proposed in [1] for problem (2.1). This method can be written as follows:

Given an initial iterate $(\xi_j^0)_{j=1,2} \in L^2(\Gamma \times (0,T))^2$, at iteration k, we solve in each subdomain $i = 1, 2$, the problem

$$\begin{aligned} \partial_t u_i^k - \Delta \varphi_i(u_i^k) &= 0, && \text{in } \Omega_i \times (0,T), \\ u_i^k(\cdot,0) &= u_0, && \text{in } \Omega_i, \\ \varphi_i(u_i^k) &= g_i && \text{on } \Gamma_i^{\mathrm{D}} \times (0,T), \\ \nabla \varphi_i(u_i^k) \cdot \mathbf{n}_i + \alpha_{ij} \Pi_i(u_i^k) &= \xi_i^{k-1} && \text{on } \Gamma \times (0,T), \end{aligned} \tag{3.6}$$

and then update the new iterates by

$$\xi_j^k = -\xi_i^{k-1} + \alpha_{ij} \pi_i(u_i^k) + \alpha_{ji} \pi_i(u_i^k).$$

The parameters α_{ij} are chosen so as to minimize the convergence factor of the linearized problem, leading to optimized parameters for a linear diffusion problem with discontinuous coefficients similar to that in [46, 50]. More precisely, the calculation of these parameters is as follows: setting $p_i = \pi_i(u_i)$, $K_i(p_i) = \lambda_i(\pi_i^{-1}(p_i))$ and $\theta_i(p_i) = \pi_i^{-1}(p_i)$, the multidomain formulation (2.2)-(2.4) also reads

$$\begin{aligned} \partial_t \left(\theta_i p_i\right) - \nabla \cdot \left(K_i(p_i) \nabla p_i\right) &= 0, && \text{in } \Omega_i \times (0,T), \\ p_1 &= p_2, && \text{on } \Gamma \times (0,T), \\ K_1(p_1) \nabla p_1 \cdot \mathbf{n}_1 &= -K_2(p_2) \nabla p_2 \cdot \mathbf{n}_2, && \text{on } \Gamma \times (0,T). \end{aligned} \tag{3.7}$$

Then the calculation of the optimized parameters is done beforehand the OSWR algorithm: we consider a linearized, frozen coefficients, version of the above problem, and calculate the parameters that minimize the convergence factor of the OSWR method applied to this linearized problem. More precisely, we approximate $\theta_i(p_i)$ by a linear function, and $K_i(p_i)$ by a constant value (e.g. the maximum value of $K_i(p_i)$). Then the optimized parameters are obtained following the methodology initiated in [49, 35] for domain decomposition in space, in [37, 51, 15, 36, 46, 17, 48] for space-time domain decomposition, and in [21] for semilinear problems. In particular, the convergence factor of the OSWR algorithm can be computed explicitly using Fourier transform, and then the optimized Robin parameters are derived by (numerically) minimizing the L^∞-norm of the convergence factor.

The well-posedness of the subdomain problem (3.3) is proved in the next section, and in section 5 the well-posedness of the discrete counterpart of the OSWR algorithm (3.5) is established, for conforming or non–conforming time discretization.

The convergence of the OSWR algorithm has been well studied for linear problems (see for instance [45, 46]). Few results exist for non-linear problems. An example for a semilinear problem is given in [21].

4. Nonlinear Robin boundary problem: existence using a finite volume discretization . In each subdomain Ω_i, $i = 1, 2$, an initial boundary value problem of type (3.3) with nonlinear Robin boundary conditions must be solved. In this section, we prove in this section that this problem has at least one solution (we do not study uniqueness, which requires more difficult methods). In this part the index i is not necessary, we change notation temporarily and consider a Robin problem in a domain $\mathcal{O} \times (0, T)$.

We thus consider a bounded domain $\mathcal{O} \subset \mathbb{R}^d$ with Lipschitz boundary. For simplicity, we assume that the Robin boundary condition is given over the whole boundary $\Gamma = \partial\mathcal{O}$, but the results can easily be extended to consider mixed boundary conditions. Given a parameter $\alpha > 0$ and Robin boundary data $\xi(\mathbf{x}, t)$ on $\Gamma \times (0, T)$, we consider the following problem: find u defined on $\mathcal{O} \times (0, T)$ such that

$$\begin{aligned} \partial_t u - \Delta\varphi(u) &= 0, && \text{in } \mathcal{O} \times (0, T), \\ \nabla\varphi(u) \cdot \mathbf{n} + \alpha\Pi(u) &= \xi(\mathbf{x}, t), && \text{on } \Gamma \times (0, T), \\ u(x, 0) &= 0, && \text{in } \mathcal{O}. \end{aligned} \tag{4.1}$$

Because the functions φ and Π that define the problem were not the primary data of the original problem, we recall the hypotheses on the data of the subdomain problem (4.1) as they will be used in the current setting.

Assumption 4.1 (Assumption on the data).

1. *The function φ is Lipschitz continuous and (strictly) increasing on $[0, 1]$, the function Π is differentiable and increasing on $[0, 1]$. Moreover, the function β defined implicitly by $\Pi = \beta \circ \varphi$ is assumed to be Lispschitz continuous with a Lispchitz constant less than 1 (cf. eq. (2.8)).*
2. *The initial data u_0 is such that $u_0 \in L^\infty(\mathcal{O})$ with $0 \le u(\mathbf{x}) \le 1$ a.e. in $\mathcal{O}$.*
3. *The Robin boundary data ξ is such that $\xi \in L^2(0, T; L^2(\Gamma))$ and the Robin parameter $\alpha > 0$ is chosen such that the following inequality is satisfied:*

$$0 < \xi(\mathbf{x}, t) < \alpha\Pi(1), \ \text{a.e. } (\mathbf{x}, t) \text{ in } \Gamma \times (0, T).$$

Remark 4.1. *Assumption 4.1–3 says that α should be chosen large enough. In the context of the OSWR algorithm, this is not a restrictive assumption. Indeed, in practice the Robin data ξ will be bounded, and a heuristic analysis for the discretization of related problems has shown that the optimized Robin parameter depends on the mesh size h like $1/h^a$ for some power $a > 0$ (see [35] and references therein for examples).*

In a first step, we define a weak solution of problem (4.1), then we propose and analyze a finite volume scheme for its approximation. The finite volume scheme will be shown to converge, and any limit will be a weak solution as in Definition 4.1.

Definition 4.1 (Weak solution for the local Robin problem). *A function u is said to be a weak solution to problem (4.1) if it satisfies:*

1. $u \in L^\infty(\mathcal{O} \times (0, T))$, $\quad 0 \le u(\mathbf{x}, t) \le 1$ *a.e. in* $\mathcal{O} \times (0, T)$,
2. $\varphi(u) \in L^2(0, T; H^1(\mathcal{O}))$,

3. *For all* $\psi \in \tilde{X} \underset{def}{=} \big\{h \in H^1(\mathcal{O}\times(0,T)),\ h(.,T)=0\big\}$,

$$
\begin{aligned}
(4.2)\quad & -\int_0^T\int_{\mathcal{O}} u(\mathbf{x},t)\partial_t\psi(\mathbf{x},t)\,d\mathbf{x}dt - \int_{\mathcal{O}} u_0\psi(\mathbf{x},0)\,d\mathbf{x} \\
& + \int_0^T\int_{\mathcal{O}} \nabla\varphi(u(\mathbf{x},t))\cdot\nabla\psi(\mathbf{x},t)\,d\mathbf{x}dt + \alpha\int_0^T\int_{\Gamma}\Pi(u(\mathbf{x},t))\psi\,d\gamma(\mathbf{x})dt \\
& = \int_0^T\int_{\Gamma}\xi(\mathbf{x},t)\psi\,d\gamma(\mathbf{x})dt,
\end{aligned}
$$

where $d\gamma(\mathbf{x})$ *is the* $(d-1)$*-dimensional Lebesgue measure on* $\partial\mathcal{O}$.

REMARK 4.2. *Because of Assumption 4.1–1, the fact that* $\varphi \in L^2(0,T,H^1(\mathcal{O}))$ *automatically implies that* $\Pi(u) \in L^2(0,T,H^1(\mathcal{O}))$*, so that* $\Pi(u)$ *has a trace on the boundary* Γ *and the last integral on the left-hand side of* (4.2) *is well defined.*

THEOREM 4.1. *Under Assumption 4.1, there exists a weak solution to problem* (4.1) *in the sense of Definition 4.1.*

The proof of Theorem 4.1 will be carried out in the rest of this section, through the study of an approximate solution defined by a finite volume method. Precisely, we prove that, if we discretize problem (4.1) using a first order finite volume scheme (see [33], [34]), then the scheme admits a unique solution (cf 4.2) that converges to a weak solution in the sense of Definition 4.1 (cf Theorem 4.2).

4.1. A space–time fully discrete approximation scheme based on finite volume in space and discontinuous Galerkin in time. We introduce here partitions of $\mathcal{O}$ and Γ, time discretization, and discrete function spaces.

4.1.1. Partitions of $\mathcal{O}$ and Γ. Let $\mathcal{T}_h$ be a partition of the subdomain $\mathcal{O}$ into elements K, such that $\overline{\mathcal{O}} = \cup_{K\in\mathcal{T}_h} K$; here we suppose that the elements are either simplices or rectangular parallelepipeds but general elements can be treated via submeshes, see [29] and the references therein. Moreover, we assume that the partition is conforming in the sense that if K, $L \in \mathcal{T}_h$, $K \neq L$, then $K \cap L$ is either an empty set, a common face, edge, or vertex of K and L.

We denote by $\mathcal{F}_h$ the set of all the faces of $\mathcal{T}_h$. The interior mesh faces in $\mathcal{T}_h$ are collected into the set $\mathcal{F}_h^{\rm int}$, whereas the faces of $\mathcal{T}_h$ lying on Γ are collected in the set $\mathcal{F}_h^{\Gamma}$. For an element $K \in \mathcal{T}_h$, we denote by $\mathcal{N}(K)$ the set of its neighbors. The notation $\mathcal{F}_K$ stands for all the faces of an element $K \in \mathcal{T}_h$, and $\mathcal{F}_{K,\Gamma} = \mathcal{F}_K \cap \mathcal{F}^{\Gamma,h}$.

For all $K \in \mathcal{T}_h$, $\mathrm{diam}(K)$ denotes the diameter of K and $|K|$ its volume. The volum of a face σ is denoted by $|\sigma|$. Finally, we use the notation $\mathbf{x}_K$ to denote the "center" of the cell $K \in \mathcal{T}_h$. If $\sigma = K|L \in \mathcal{F}_h$ separates the cells K and L, $d_{K,L}$ denotes the Euclidean distance between $\mathbf{x}_K$ and $\mathbf{x}_L$, and $d_{K,\sigma}$ for $\sigma \in \mathcal{F}_K$ denotes the distance from $\mathbf{x}_K$ to σ. For $\sigma \in \mathcal{F}_K$, we denote by $\tau_{K,\sigma}$ the transmissivity of K through σ, given by $\tau_{K,\sigma} = \frac{|\sigma|}{d_{K,\sigma}}$. If $\sigma = K|L$, we use $\tau_{K,L} = \frac{|\sigma|}{d_{K,L}}$.

We assume that the mesh $\mathcal{T}_h$ satisfies the following orthogonality condition (see [33]): for an interface $\sigma = K|L$, the line segment $\mathbf{x}_K\mathbf{x}_L$ is orthogonal to this interface (see Fig. 4.1).

The size of the mesh is defined by

$$
(4.3)\qquad \mathrm{size}(\mathcal{T}) = \max_{K\in\mathcal{T}} \mathrm{diam}(K),
$$

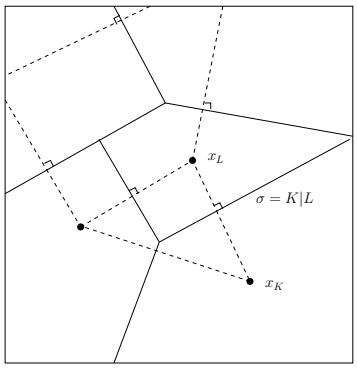

FIG. 4.1. *Notation for admissible meshes in two space dimensions*

and the regularity measure of the mesh is defined by

$$\mathrm{reg}(\mathcal{T}) = \max_{K\in\mathcal{T}} \Big(\max_{\sigma\in\mathcal{F}_K} \frac{\mathrm{diam}(K)}{d_{K,\sigma}} \Big). \tag{4.4}$$

4.1.2. Time discretization. For an integer $M \geq 0$, let $(\tau^n)_{0\leq n\leq M}$ denote a sequence of positive real numbers corresponding to the discrete time steps such that $T = \sum_{n=1}^{M} \tau^n$. Let $t^0 = 0$, and $t^n = \sum_{j=1}^{n} \tau^j$, $1 \leq n \leq M$, be the discrete times. Let $J^n = (t^{n-1}, t^n]$, $1 \leq n \leq M$. We denote the time discretization by $\mathcal{M} = \{J^n, 1 \leq n \leq M\}$ and we let $\tau_{\mathcal{M}} = \max_{0\leq n\leq M} \tau^n$.

4.1.3. Discrete function spaces. Given a partition $\mathcal{T}_h$ of $\mathcal{O}$ and a time discretization $\mathcal{M}$ satisfying the conditions listed in subsection 4.1.1 and subsection 4.1.2, we say that $\mathcal{D} = (\mathcal{T}_h, \mathcal{M})$ is an *admissible space–time discretization* of $\mathcal{O}\times(0,T)$. We then denote $\mathrm{size}(\mathcal{D}) = \max(\mathrm{size}(\mathcal{T}_h), \tau)$ and $\mathrm{reg}(\mathcal{D}) = \mathrm{reg}(\mathcal{T}_h)$.

DEFINITION 4.2. *Let $\mathcal{D}$ be an admissible discretization of $\mathcal{O}\times(0,T)$. We denote by $\mathcal{X}(\mathcal{D})$ the functional space of piecewise constant functions $u_{\mathcal{D}}$ defined on $\mathcal{O}\times(0,T)$:*

$$\mathcal{X}(\mathcal{D}) = \big\{ u_{\mathcal{D}} : \mathcal{O}\times(0,T) \to \mathbb{R} \ s.t \text{ for all } (K,J) \in \mathcal{T}\times\mathcal{M}, \ u_{\mathcal{D}} \text{ is constant on } K\times J \big\}. \tag{4.5}$$

Functions in $\mathcal{X}(\mathcal{D})$ have a trace on Γ, and the trace operator $\overline{\gamma}$ is defined, for $u_{\mathcal{D}} \in \mathcal{X}(\mathcal{D})$, by $\overline{\gamma}(u) = u_\sigma$ for $\sigma \in \mathcal{F}_h^\Gamma$.

Finally, the space $\mathcal{X}(\mathcal{D})$ will be endowed with the discrete $L^2(0,T;H^1(\mathcal{O}))$-seminorm defined, for $u \in \mathcal{X}(\mathcal{D})$ by

$$|u|_{1,\mathcal{D}}^2 = \sum_{n=0}^{M} \tau^n \sum_{\sigma\in\mathcal{F}} \tau_{K,\sigma} |D_\sigma u|^2 \tag{4.6}$$

where $D_\sigma u = (u_K - u_L)$ if $\sigma \in \mathcal{F}_{int}$, $\sigma = K|L$ and $D_\sigma u = (u_K - u_\sigma)$ if $\sigma \in \mathcal{F}_{K,\Gamma}$.

REMARK 4.3. *Functions in $\mathcal{D}$ have a natural identification with functions in the following space*

$$P_0(\mathcal{M},\mathcal{T}) = \big\{ u : (0,T) \to L^2(\mathcal{O}), \ s.t. \text{ for all } J \in \mathcal{M}, u(t) \text{ is constant on } J \text{ with value in the space of functions piecewise constant on } \mathcal{T} \big\}$$

4.1.4. The fully discrete scheme. In order to obtain a finite volume discretization of problem (4.1), we integrate as usual the first equation on each cell of the mesh. The initial condition u_K^0 is given by

$$u_K^0 = \frac{1}{|K|}\int_K u_0 \,\mathrm{d}\mathbf{x}, \ \forall K \in \mathcal{T}. \tag{4.7}$$

For the following time steps we compute a discrete solution $\Big(\big(u_K^{n+1}\big)_{K\in\mathcal{T}}, \big(u_\sigma^{n+1}\big)_{\sigma\in\mathcal{F}_h^\Gamma}\Big)$, for all $n \in \{0,\dots,M-1\}$, thanks to the scheme defined by

$$\begin{aligned} |K|\frac{u_K^{n+1}-u_K^n}{\tau^n} &+ \sum_{L\in\mathcal{N}(K)} \tau_{K,L}\Big(\varphi(u_K^{n+1}) - \varphi(u_L^{n+1})\Big) \\ &+ \sum_{\sigma\in\mathcal{F}_{K,\Gamma}} \tau_{K,\sigma}\Big(\varphi(u_K^{n+1}) - \varphi(u_\sigma^{n+1})\Big) = 0, \quad \forall K \in \mathcal{T}, \end{aligned} \tag{4.8}$$

$$-\tau_{K,\sigma}\Big(\varphi(u_K^{n+1}) - \varphi(u_\sigma^{n+1})\Big) + \alpha|\sigma|\Pi(u_\sigma^{n+1}) = \xi_\sigma^{n+1}, \quad \forall \sigma \in \mathcal{F}_h^\Gamma \cap \mathcal{F}_K \tag{4.9}$$

where we set for all $\sigma \in \mathcal{F}_h^\Gamma$

$$\xi_\sigma^{n+1} = \frac{1}{\tau^n}\int_{J^n}\int_\sigma \xi(\mathbf{x},t)\,\mathrm{d}\gamma(\mathbf{x})\,\mathrm{d}t.$$

An approximate solution $u_\mathcal{D} \in \mathcal{X}(\mathcal{D})$ to the problem (4.1) associated to the discretization $\mathcal{D}$ is defined by

$$u_\mathcal{D}(\mathbf{x},t) = \begin{cases} u_K^{n+1}, & \forall \mathbf{x} \in K,\ K \in \mathcal{T}, \\ u_\sigma^{n+1}, & \forall \mathbf{x} \in \sigma,\ \sigma \in \mathcal{F}_h^\Gamma, \end{cases} \qquad \forall t \in J,\ \forall J \in \mathcal{M},$$

where $u_\mathcal{D}$ is a solution of (4.7)–(4.9).

Let us emphasize that the discretization of the problem with a Robin boundary condition is performed with the help of additional unknowns that are defined on the edges of the boundary Γ. These may be eliminated when solving the resulting system (see Lemma 4.1). In most of the estimates to be presented, we shall usually keep them because they simplify the presentation of the results, with the understanding that they are functions of the interior unknowns.

4.2. Well-posedness and L^∞-stability of the scheme. This subsection is devoted to a proof that the finite volume scheme admits a unique solution that is moreover in $[0,1]^N$.

Because the proof will use Brouwer's fixed point theorem, we begin by recasting the finite volume scheme in a fixed point form. We start with a technical lemma that will allow us to eliminate the boundary unknowns whenever necessary.

LEMMA 4.1. *Under Assumption 4.1–3, for all $K \in \mathcal{T}$, for all $n \in \{0,\dots,M-1\}$, and for all $u_K^{n+1} \in \mathbb{R}$, there exists a unique $u_\sigma^{n+1} \in [0,1]$ solution of (4.9).*

Proof. Equation (4.9) may be rewritten as

$$\tau_{K,\sigma}\varphi(u_\sigma^{n+1}) + \alpha|\sigma|\Pi(u_\sigma^{n+1}) = \xi_\sigma^{n+1} + \tau_{K,\sigma}\varphi(u_K^{n+1}). \tag{4.10}$$

For $\alpha > 0$, the function $\theta : s \longmapsto \tau_{K,\sigma}\varphi(s) + \alpha|\sigma|\Pi(s)$ is strictly increasing on $[0,1]$, ensuring the uniqueness of the solution of (4.10). Moreover,

$$\theta(0) = 0, \quad \theta(1) = \tau_{K,\sigma}\varphi(1) + \alpha|\sigma|\Pi(1).$$

Now, using Assumption 4.1, we have $\theta(0) < \xi_\sigma^{n+1} + \tau_{K,\sigma}\varphi(u_K^{n+1}) < \theta(1)$, for any $u_K^{n+1} \in \mathbb{R}$. Existence then follows from the intermediate value theorem. ∎

We can now give the fixed point form of the finite volume scheme (4.8)—(4.9).

It will be convenient to temporarily denote the set of discrete unknowns at time t^n, for a fixed n, by $U^n = ((u_l)_{L\in\mathcal{T}})$. After adding and substracting the term $\lambda_K u_K^{n+1}$ to equation (4.8), where λ_K is given on each cell by:

$$\lambda_K = \frac{\tau^n L_\varphi}{|K|}\Big(\sum_{L\in\mathcal{N}(K)} \tau_{K,L} + \sum_{\sigma\in\mathcal{F}_{K,\Gamma}} \tau_{K,\sigma}\Big)$$

(we justify this choice during the proof of Proposition 4.1 below), we see that system (4.8)–(4.9) is equivalent to

$$U^{n+1} = H(U^n, U^{n+1}) \tag{4.11}$$

where, for each $K \in \mathcal{T}$, $(H(U^n, U^{n+1}))_K = H_K(u_K^n, U^{n+1})$ is given by

$$\begin{aligned} H_K(u_K^n, U) = \frac{1}{1+\lambda_K}\Bigg(u_K^n + \lambda_K u_K + \frac{\tau^n}{|K|}\sum_{L\in\mathcal{N}(K)} \tau_{K,L}\Big(\varphi(u_L) - \varphi(u_K)\Big) \\ + \frac{\tau^n}{|K|}\sum_{\sigma\in\mathcal{F}_{K,\Gamma}} \tau_{K,\sigma}\Big(\varphi(u_{K,\sigma}) - \varphi(u_K)\Big)\Bigg), \end{aligned} \tag{4.12}$$

and we recall that $u_{K,\sigma} = \theta^{-1}(u_K)$ is a function of u_K via Lemma 4.1.

Proposition 4.1. *The following properties hold for the mapping H:*

1. *H is a non-decreasing function of each of its arguments,*
2. *H maps $[0,1]\times[0,1]^N$ to $[0,1]^N$,*

Proof. To prove the first assertion, let $U = (u_L)_{L\in\mathcal{T}}$ and $V = (v_L)_{L\in\mathcal{T}}$ be two grid functions such that $u_L \le v_L$, $\forall L \in \mathcal{T}$. We make use of the definition of λ_K to write

$$\begin{aligned} &(1+\lambda_K)\left(H_K(u_K^n, U) - H_K(u_K^n, V)\right) \\ &\quad = \lambda_K(u_K - v_K) + \frac{\tau^n}{|K|}\sum_{L\in\mathcal{N}(K)} \tau_{K,L}(\varphi(u_L) - \varphi(v_L)) \\ &\qquad + \frac{\tau^n}{|K|}\sum_{\sigma\in\mathcal{E}_{K,\Gamma}} \tau_{K,\sigma}(\varphi(u_{K,\sigma}) - \varphi(v_{K,\sigma})) + \frac{\lambda_K}{L_\varphi}\left(\varphi(v_K) - \varphi(u_K)\right). \end{aligned}$$

As φ is increasing, the second and third terms on the right hand side are negative (for the third term, we also use that θ^{-1} is increasing), and we can bound the last term by $\lambda_K(v_K - u_K)$, so that the left-hand side is negative. The monotonicity of H with respect to its first argument is obvious.

For the second assertion, we rewrite $H_K(u_K^n, U)$ in the form

$$\begin{aligned} (1+\lambda_K)H_K(u_K^n, U) = u_K^n + \sum_{L\in\mathcal{N}(K)} a_{KL}\, u_L + \sum_{\sigma\in\mathcal{F}_{K,\Gamma}} a_{K\sigma}\, u_\sigma \\ + \left(\lambda_K - \sum_{L\in\mathcal{N}(K)} a_{KL} - \sum_{\sigma\in\mathcal{F}_{K,\Gamma}} a_{K\sigma}\right) u_K \end{aligned}$$

where we have defined

$$a_{KL} = \frac{\tau^n}{|K|} \sum_{L \in \mathcal{N}(K)} \tau_{KL} \frac{\varphi(u_L) - \varphi(u_K)}{u_L - u_K}$$

and

$$a_{K\sigma} = \frac{\tau^n}{|K|} \sum_{\sigma \in \mathcal{F}_{K,\Gamma}} \tau_{K\sigma} \frac{\varphi(u_\sigma) - \varphi(u_K)}{u_\sigma - u_K}.$$

Because φ is increasing, the quantities a_{KL} and $a_{K\sigma}$ are all positive, and because of the choice for λ_K, $\lambda_K - \sum_{L \in \mathcal{N}(K)} a_{KL} - \sum_{\sigma \in \mathcal{F}_{K,\Gamma}} a_{K\sigma}$ is also positive, so that $H_K \geq 0$, $\forall K \in \mathcal{T}$. On the other side, by the monotonicty of H proven in the first assertion,

$$H_K(u_K, (u_L)_{L\in\mathcal{T}}) \leq H_K(1, (1)_{L\in\mathcal{T}}) \leq \frac{1}{1+\lambda_K} \left(1 + \sum_{L \in \mathcal{N}(K)} a_{KL} + \sum_{\sigma \in \mathcal{F}_{K,\Gamma}} a_{K\sigma} + \lambda_K - \sum_{L \in \mathcal{N}(K)} a_{KL} - \sum_{\sigma \in \mathcal{F}_{K,\Gamma}} a_{K\sigma} \right) = 1.$$

This completes the proof. ∎

We can now state and prove an existence and uniqueness result for the scheme.

PROPOSITION 4.2. *Let assumptions 2.1 and 4.1 hold. Let $\mathcal{D}$ be an admissible discretization of $\mathcal{O} \times (0,T)$. There exists a discrete solution $u_\mathcal{D} \in \mathcal{X}(\mathcal{D})$ to the scheme (4.7)–(4.9) such that*

$$0 \leq u_\mathcal{D} \leq 1, \quad \text{almost everywhere in } \mathcal{O} \times (0,T). \tag{4.13}$$

Proof. By Lemma 4.1, we only need to prove the result for the interior unknowns. We prove the existence and the uniqueness of $\left(u_K^{n+1}\right)_{K\in\mathcal{T}}$ by induction on n. This is clear for $n = 0$, as the initial saturation $\left(u_K^0\right)_{K\in\mathcal{T}}$ is given by (4.7).

For the induction step, let us suppose now that for some $n \in \mathcal{M}$, the set $(u_K^n)_{K\in\mathcal{T}} \in [0,1]^N$ is known, and we need to prove the existence and the uniqueness of $\left(u_K^{n+1}\right)_{K\in\mathcal{T}}$ as solution of the fixed-point equation (4.11).

Existence: This follows from a straightforward application of Brouwer's fixed point theorem (see [28, thm 9.9.2] or [53, thm 6.3.2]). Indeed, by Proposition 4.1, and since u_K^n is in $[0,1]$ for all $K \in \mathcal{T}$, H maps the compact and convex set $[0,1]^N$ to itself, and is obviously continuous, hence admits a fixed point in the same set, as stated in (4.13).

Uniqueness: The proof follows exactly that in [31, Proposition 2.8], and uses the monotonicity of the mapping H. ∎

4.3. Convergence analysis of the scheme. The aim of this subsection is to prove that the solution of the finite volume scheme defined in the previous section converges to a limit that is a weak solution of problem (4.1)

THEOREM 4.2. *Let assumptions 2.1 and 4.1 hold. Let $(\mathcal{D}_m)_m$ be a sequence of admissible discretizations of $\mathcal{O} \times (0,T)$ and denote by $u_m = u_{\mathcal{D}_m}$ the approximate*

solution of the finite volume scheme (4.8), (4.9). There exists $u \in L^\infty(\mathcal{O}\times(0,T))$ *such that, if* $\lim_{m\to\infty} \mathrm{size}(\mathcal{D}_m) = 0$, *and if there exists* $\zeta > 0$ *such that* $\mathrm{reg}(\mathcal{D}_m) \le \zeta$, *then (up to a subsequence)*

$$u_m \to u \in L^p(\mathcal{O}\times(0,T)), \quad \forall p \in [1,\infty),$$

and u *is a weak solution to problem (4.1) in the sense of Definition 4.1*

The proof will be broken down in several steps, following a now classical strategy, see [33], and also [22, 23, 24, 31]: we first prove some a priori estimates in subsection 4.3.1, so as to show that the discrete solution lies in a bounded set in $L^2(0,T;H^1(\mathcal{O}))$. Then, in subsection 4.3.2, we use a result from [12] to pass to the limit in the non-linear terms. Last, in subsection 4.3.3, we prove that the limit is a weak solution of problem (4.1).

4.3.1. Energy estimate. We now prove the following energy estimate.

PROPOSITION 4.3 (discrete $L^2(0,T;H^1(\mathcal{O}))$ estimate). *Let* $\mathcal{D}$ *be an admissible discretization of the domain* $\mathcal{O}\times(0,T)$. *Let* $u_\mathcal{D}$ *be the solution given by the scheme (4.8)–(4.9). There exists a constant* C *such that*

$$|\varphi(u_\mathcal{D})|_{1,\mathcal{D}} + ||\overline{\gamma}(\Pi(u_\mathcal{D}))||_{L^2(\Gamma\times(0,T))} \le C, \tag{4.14}$$

where $\overline{\gamma}(u_\mathcal{D})$ *stands for the trace of* $u_\mathcal{D}$ *on* Γ *as in Definition 4.2.*

Proof (cf. prop. 2.5 in [22]). Multiplying (4.8) by $\tau^n\varphi(u_K^{n+1})$ and (4.9) by $\tau^n\varphi(u_\sigma^{n+1})$ then summing over all cells, all boundary faces and all time steps gives, after a discrete intergration by parts

$$\begin{aligned}\sum_{n=0}^{M}\Bigg[\sum_{K\in\mathcal{T}}|K|\Big(u_K^{n+1}-u_K^n\Big)\varphi(u_K^{n+1}) + \tau^n\sum_{\substack{\sigma\in\mathcal{F}_{int}\\ \sigma=K|L}}\tau_{K,L}|\varphi(u_K^{n+1})-\varphi(u_L^{n+1})|^2 \\ + \tau^n\sum_{\substack{\sigma\in\mathcal{F}_h^\Gamma\\ \mathcal{F}_{K,\Gamma}\ni\sigma}}\tau_{K,\sigma}|\varphi(u_K^{n+1})-\varphi(u_\sigma^{n+1})|^2 + \tau^n\sum_{\sigma\in\mathcal{F}_h^\Gamma}\alpha|\sigma|\Pi(u_\sigma^{n+1})\varphi(u_\sigma^{n+1})\Big)\Bigg] \\ = \sum_{n=0}^{M}\tau^n\sum_{\sigma\in\mathcal{F}_\Gamma}\xi_\sigma^{n+1}\varphi(u_\sigma^{n+1}).\end{aligned} \tag{4.15}$$

Since φ is an increasing function, the function $f: s\mapsto\int_0^s\varphi(a)\,da$ is convex, so that

$$f(u_K^n) + \varphi(u_K^{n+1})\Big(u_K^{n+1}-u_K^n\Big) \ge f(u_K^{n+1}).$$

Thus

$$\begin{aligned}\sum_{n=0}^{M}\sum_{K\in\mathcal{T}}|K|\Big(u_K^{n+1}-u_K^n\Big)\varphi(u_K^{n+1}) &\ge \sum_{K\in\mathcal{T}}|K|\Big(f(u_K^{M+1})-f(u_K^0)\Big) \\ &\ge -|\mathcal{O}|\int_0^1\varphi(a)\,da.\end{aligned} \tag{4.16}$$

Now, using (2.8) and the fact that $\varphi(0)=0$ and $\Pi(0)=0$ we obtain

$$\alpha\sum_{n=0}^{M}\tau^n\sum_{\sigma\in\mathcal{F}_\Gamma}|\sigma|\Pi(u_\sigma^{n+1})\varphi(u_\sigma^{n+1}) \ge \alpha\sum_{n=0}^{M}\tau^n\sum_{\sigma\in\mathcal{F}_\Gamma}|\sigma||\Pi(u_\sigma^{n+1})|^2.$$

Inserting this estimate together with (4.16) in (4.15), one gets (4.14) in the form

$$|\varphi(u_{\mathcal{D}})|^2_{1,\mathcal{D}} + \alpha||\overline{\gamma}(\Pi(u_{\mathcal{D}}))||^2_{L^2(\Gamma\times(0,T))} \leq |\mathcal{O}| \int_0^1 \varphi(a)\, da + \varphi(1) \int_0^T \int_\Gamma \xi(\mathbf{x},t) \mathrm{d}\gamma(\mathbf{x}) \mathrm{d}t.$$

∎

4.3.2. Application of compactness results. We want to apply the compactness results stated in [12, Theorem 3.9].

First we check the "structural assumptions" on the scheme.

Assumption (Ax1) This is well known for the two–point flux approximation scheme used here. The proof can be found in [33, Lemma 9.3].

Assumption (Ax2) Trivial here, as the scheme uses piecewise constant functions;

Assumption (Ax3) It is shown in [12] that Assumption (**Ax3**) holds;

Assumption (At) Always true for one–step scheme.

In addition to the energy estimate proven in Proposition 4.3, we need a result on the time derivative of the discrete solution. This is proved in the following Lemma (cf [3, Lemma 4.1] or [4, Lemma 4.1]).

LEMMA 4.2. *Let $\mathcal{D}$ be an admissible discretization of $\mathcal{O}\times(0,T)$. If Assumptions Assumption 4.1 hold, there exists a constant C such that, for all $\psi \in C_c^\infty(\mathcal{O}\times(0,T))$, there holds:*

$$\sum_{n=0}^{M} \tau^n \sum_{K\in\mathcal{T}} |K| \frac{u_K^{n+1}-u_K^n}{\tau^n} \psi_K^{n+1} \leq C\|\nabla\psi\|_{L^\infty(\mathcal{O}\times(0,T))}, \tag{4.17}$$

where we have let $\psi_K^{N=1} = \psi(x_K, t^{n+1})$.

Proof. We proceed as in the proof of Proposition 4.3, multiplying eq. (4.8) by $\tau^n\psi_K^{n+1}$, and summing over all elements and all time steps . This time there are no boundary terms, because ψ vanishes on the boundary of $\mathcal{O}$, and after a discrete integration by parts we obtain $A = B$ with

$$A = \sum_{n=0}^{M} \sum_{K\in\mathcal{T}} |K|(u_K^{n+1}-u_K^n)\psi_K^{n+1}, \tag{4.18}$$

$$B = \sum_{n=0}^{M} \tau^n \sum_{\substack{\sigma\in\mathcal{F}\\ \sigma=K|L}} \tau_\sigma \left(\varphi(u_K^{n+1}) - \varphi(u_L^{n+1})\right)\left(\psi_K^{n+1} - \psi_L^{n+1}\right). \tag{4.19}$$

We now bound B using the Cauchy–Schwarz inequality:

$$|B|^2 \leq B_1 B_2$$

where

$$B_1 = \sum_{n=0}^{M} \tau^n \sum_{\substack{\sigma\in\mathcal{F}\\ \sigma=K|L}} \tau_\sigma \left(\varphi(u_K^{n+1}) - \varphi(u_L^{n+1})\right)^2, \text{ and } B_2 = \sum_{n=0}^{M} \tau^n \sum_{\substack{\sigma\in\mathcal{F}\\ \sigma=K|L}} \tau_\sigma (\psi_K^{n+1} - \psi_L^{n+1})^2.$$

Thanks to Proposition 4.3 we know that B_1 is bounded by a constant, while

$$B_2 \leq \left(\sum_{n=0}^{M} \tau^n \sum_{\substack{\sigma\in\mathcal{F}\\ \sigma=K|L}} \tau_\sigma d_{KL}\right) \|\nabla\psi\|^2_{L^\infty(\mathcal{O}\times(0,T))}.$$

Finally

$$\sum_{n=0}^{M} \tau^n \sum_{\substack{\sigma\in\mathcal{F}\\ \sigma=K|L}} \tau_\sigma d_{KL} \le T \sum_{\substack{\sigma\in\mathcal{F}\\ \sigma=K|L}} \tau_\sigma d_{KL},$$

and the last term in bounded by a constant depending only on $\mathcal{O}$ and the space dimension. ∎

We are now able to use [12, Thm. 3.9], and obtain the following result

PROPOSITION 4.4. *Up to a subsequence, $\varphi(u_m)$ converges in $L^2(\mathcal{O}\times(0,T))$ towards $\varphi(u)$. Moreover, the limit function $\varphi(u)$ is actaullay in $L^2(0,T;H^1(\mathcal{O}))$.*

Proof. Only the last assertion remains to be proved. This result is a standard consequence of Assumption **Ax1**, and was proved in [31, Thm. 2.15]. ∎

There now remains to prove the convergence of the trace. Note that it known that, because β is Lipschitz, $\Pi(u)=\beta(\varphi(u))$ is in $L^2(0,T;H^1(\mathcal{O}\times(0,T)))$ (cf. [10, Cor.3.2]). Thus the trace of $\Pi(u)$ is well defined.

LEMMA 4.3. *Up to a subsequence, the sequence $\left(\Pi(u_{\mathcal{D}_m|\Gamma})\right)_m$ converges weakly towards $\Pi(u)$ in $L^2(\Gamma\times(0,T))$.*

Proof. The convergence in $L^2((0,T)\times\mathcal{O})$ of the sequence $(\varphi(u_{\mathcal{D}_m}))_m$ together with the bound (4.14) on the gradients shows that, up to a subsequence, the sequence actually converges weakly in $L^2((0,T);H^1(\mathcal{O}))$ toward $\varphi(u)$. Because $\Pi=\beta\circ\varphi$, with a Lipschitz continuous function β, the same result is true if we replace φ by Π. By continuity of the trace operator, we obtain the weak convergence of $\left(\Pi(u_{\mathcal{D}_m|\Gamma})\right)_m = (\bar\gamma(\Pi(u_m)))_m$ towards $\bar\gamma(\Pi(u))$ in $L^2((0,T)\times\Gamma$.

Finally we can prove the convergence of $\mathcal{D}_m$ as stated in Theorem 4.2.

COROLLARY 4.1. *Up to a subsequence, $(u_m)_m$ converges towards u strongly in $L^p(\Omega\times(0,T))$ for all $p\in[1,\infty)$.*

Proof. Since $(\varphi(u_m))_m$ converges in $L^2(\mathcal{O}\times(0,T))$ towards $\varphi(u)$, it converges (up to a new subsequence) almost everywhere in $\Omega\times(0,T)$. The fact that φ^{-1} is continuous, implies that $(u_m)_m$ tends to u almost everywhere. We conclude using the uniform bound on $(\varphi(u_m))_m$ stated in Proposition 4.2. ∎

4.3.3. Existence of a weak solution. We now have all the elements to finish the proof of Theorem 4.2. We have shown previously that u_m converge toward u as $m\to\infty$. Moreover, it has been stated in Proposition Lemma 4.3 that $(\overline{\gamma}(\Pi(u_m)))_m$ converges towards $\overline{\gamma}\left(\Pi(u)\right)$ weakly in $L^2(\Gamma\times(0,T))$. It remains to verify that u satisfy the weak formulation in the sense of Definition 4.1.

Let $\psi\in\tilde{U}_{test}=\left\{h\in C^2(\overline{\Omega}\times(0,T)),\ h(.,T)=0\right\}$ and, for $m\in\mathbb{N}$, let u_m be given by (4.8), (4.9) for the admissible discretization $\mathcal{D}_m$. For all $n\in\{0,\dots,M-1\}$ and for all $K\in\mathcal{T}$, we multiply (4.8) by $\psi_K^n=\psi(\mathbf{x}_K,n\tau^n)$, and (4.9) by $\psi_\sigma^n=\psi(\mathbf{x}_\sigma,n\tau^n)$ then sum over cells, all faces and over $n\in\mathcal{M}$ to obtain

$$\sum_{i=1}^{4} T_{i,m} = G_m,$$

where

$$T_{1,m} = \sum_{n=0}^{M} \sum_{K\in\mathcal{T}} |K|\Big(u_K^{n+1} - u_K^{n+1}\Big)\psi_K^n,$$

$$T_{2,m} = \sum_{n=0}^{M} \tau^n \sum_{L\in\mathcal{N}(K)} \tau_{K,L}\Big(\varphi(u_K^{n+1}) - \varphi(u_L^{n+1})\Big)\psi_K^n,$$

$$T_{3,m} = \sum_{n=0}^{M} \tau^n \sum_{\sigma\in\mathcal{F}_{K,\Gamma}} \tau_{K,\sigma}\Big(\varphi(u_K^{n+1}) - \varphi(u_\sigma^{n+1})\Big)\Big(\psi_K^n - \psi_\sigma^n\Big),$$

$$T_{4,m} = \sum_{n=0}^{M} \tau^n \sum_{\sigma\in\mathcal{F}_{K,\Gamma}} \alpha|\sigma|\Pi(u_\sigma^{n+1})\psi_\sigma^n,$$

$$G_m = \sum_{n=0}^{M} \tau^n \sum_{\sigma\in\mathcal{F}_{K,\Gamma}} \xi_\sigma^{n+1}\psi_\sigma^n.$$

We follow [33, Proof of Thm. 4.2], see also [31] and the references therein, to obtain

$$\lim_{m\to\infty} T_{1,m} = -\int_0^T \int_{\mathcal{O}} u(\mathbf{x},t)\partial_t\psi(\mathbf{x},t)\,\mathrm{d}\mathbf{x}\mathrm{d}t - \int_{\mathcal{O}} u_0\psi(\mathbf{x},0)\,\mathrm{d}\mathbf{x}.$$

Still following [31], summing the terms by edges in $T_{2,m}$, we obtain

$$T_{2,m} = \sum_{n=0}^{M} \tau^n \sum_{\sigma=L|K\in\mathcal{T}_{int}} \tau_{K,L}\Big(\varphi(u_K^{n+1}) - \varphi(u_L^{n+1})\Big)\left(\psi_K^n - \psi_L^{n+1}\right),$$

and then

$$\lim_{m\to\infty} T_{2,m} = \int_0^T \int_{\mathcal{O}} \nabla\varphi(u(\mathbf{x},t))\cdot\nabla\psi(\mathbf{x},t)\,\mathrm{d}\mathbf{x}\mathrm{d}t.$$

Now, we apply the Cauchy-Schwarz inequality to $T_{3,m}$ to obtain

$$\begin{aligned} T_{3,m}^2 \le & \Big(\sum_{n=0}^{M} \tau^n \sum_{\sigma\in\mathcal{F}_{K,\Gamma}} \tau_{K,\sigma}\Big(\varphi(u_K^{n+1}) - \varphi(u_\sigma^{n+1})\Big)^2\Big) \\ & \times\Big(\sum_{n=0}^{M} \tau^n \sum_{\sigma\in\mathcal{F}_{K,\Gamma}} |\sigma|\frac{\Big(\psi_K^n - \psi_\sigma^n\Big)^2}{d_{K,\sigma}}\Big). \end{aligned} \tag{4.20}$$

The first term in the product is bounded, because of (4.14). Let C_ψ denote the Lipschitz constant of ψ. We obtain using (4.4)

$$\sum_{n=0}^{M} \tau^n \sum_{\sigma\in\mathcal{F}_{K,\Gamma}} |\sigma|\frac{\Big(\psi_K^n - \psi_\sigma^n\Big)^2}{d_{K,\sigma}} \le 4T|\Gamma|C_\psi^2\,\mathrm{size}(\mathcal{M}).$$

Hence,

$$\lim_{m\to\infty} T_{3,m} = 0.$$

Finally, using Lemma 4.3, and thanks to the regularity of the function ψ, we obtain

$$\lim_{m\to\infty} T_{4,m} = \alpha\int_0^T \int_\Gamma \Pi(u(\mathbf{x},t))\psi\,\mathrm{d}\gamma(\mathbf{x})\mathrm{d}t.$$

Similarly,

$$\lim_{m\to\infty} G_m = \int_0^T \int_\Gamma \xi(\mathbf{x},t)\psi \,\mathrm{d}\gamma(\mathbf{x})\mathrm{d}t.$$

This ends the proof of Theorem 4.2, and together with Proposition 4.2 also proves Theorem 4.1.

REMARK 4.4. *It is worth noticing that uniqueness of the weak solution in the sense of Definition 4.1 could be obtained using entropy inequalities, obtained through the method of doubling variables [34, 13] (see also [23] for the case of Neumann boundary conditions). Given the length of the paper, this task will not be pursued.*

5. Multidomain formulation and OSWR algorithm in the discrete case. The aim of this section is to design and analyze a discrete version of the multidomain formulation (2.9)–(3.1) (or equivalently (3.4)), and of the OSWR algorithm (3.6). This global-in-time algorithm together with discontinuous Galerkin (DG) for the time discretization allows for the use of different time steps in different subdomains, and has been analyzed for linear problems in [44, 45], and also [17, 42, 46] for porous media applications.

We first present the discrete multidomain problem with nonconforming time grids, and the the OSWR algorithm to solve this problem. We show that in the particular case of matching time grids, the discrete multidomain problem is equivalent to the one in [31].

Notation for the space discretization. We extend the notation of section 4 to the multidomain case by simply adding a subscript or a superscript denoting the subdomain index to the corresponding entity (e.g. $\mathcal{M}_i$ denotes the set of all time intervals in sudomain Ω_i). Let $\mathcal{D}_i$ be an admissible discretization of $\Omega_i \times (0,T)$ as in subsection 4.1.3. The respective spatial meshes are supposed to be matching on the interface Γ: $\mathcal{F}_\Gamma^1 = \mathcal{F}_\Gamma^2$. Then, we define the admissible composite discretization

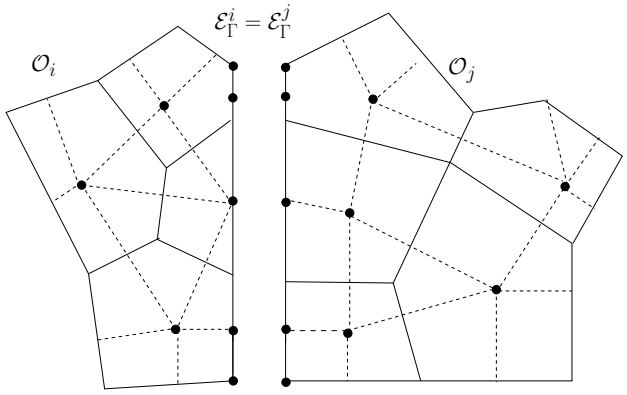

FIG. 5.1. *Partition of the domain with conforming space grids.*

associated with $\Omega \times (0,T)$

DEFINITION 5.1 (Admissible space–time discretization of $\Omega \times (0,T)$). *Let $\mathcal{D}_i$ be an admissible discretization of $\Omega_i \times (0,T)$. A composite discretization $\mathcal{D}$ of $\Omega \times (0,T)$ is given by $\mathcal{D} = (\mathcal{T}, \mathcal{F}_\Gamma, \mathcal{P}, \mathcal{M})$, where $X = \cup_{i\in\{1,2\}} X_i$, for $X = \mathcal{T}, \mathcal{F}_\Gamma, \mathcal{P}, \mathcal{M}$.*

Time projections. On the space–time interface $\Gamma \times (0,T)$ we define the following L^2 projection $\mathcal{P}_{ij}$ from $P^0(\mathcal{M}_j, L^2(\Gamma_j))$ to $P^0(\mathcal{M}_i, L^2(\Gamma_i))$, as follows:

For $\psi \in P^0(\mathcal{M}_j, L^2(\Gamma_j))$,

$$(\mathcal{P}_{ij}\psi)_{|J_i^n} = \frac{1}{\delta t_i} \sum_{m=1}^{M_j} \int_{J_i^n \cap J_j^m} \psi \, dt, \qquad \text{for all } n \in \{0, \dots, M_i\}. \tag{5.1}$$

These time projections are used to transfer data from one space–time subdomain to a neighboring subdomain, and are obtained by a projection algorithm with linear complexity and without any additional grid, see [38, 39].

5.1. Discrete multidomain problem with nonconforming time grids. In this section the partitions $\mathcal{M}_i$, $i = 1, 2$, are generated independently, with respect to the physical characteristics of each subdomain. For simplicity, the partition $\mathcal{M}_i$ is supposed uniform, with sub-intervals $J_i^n = (t_i^n, t_i^{n+1}]$, and time step $\tau_i = t_i^{n+1} - t_i^n$, as shown in Figure 5.2.

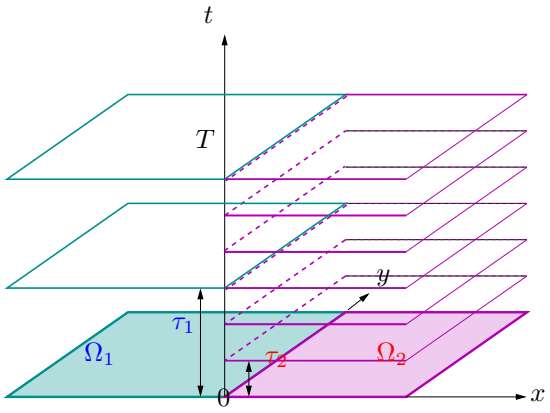

FIG. 5.2. *Nonconforming time grids in the subdomains.*

For a given discretization $(\mathcal{M}, \mathcal{T})$, it will be convenient to define (see Remark 4.3) for any function $\xi \in P_0(\mathcal{M}, \mathcal{T})$,

$$\xi_K(t) = \xi_K^n, \text{ for } t \in J^n, \text{ and } K \in \mathcal{T}. \tag{5.2}$$

The discrete counterpart of the subproblem problem (2.9)–(3.1) is as follows: for $i = 1, 2$, the initial condition is given by

$$u_K^0 = \frac{1}{|K|} \int_K u_0 \, \mathrm{d}\mathbf{x}, \ \forall K \in \mathcal{T}_i, \tag{5.3a}$$

and for $n = 0, \dots, M_i - 1$, the discrete saturations $\left(\left(u_K^{n+1}\right)_{K \in \mathcal{T}_i}, \left(u_\sigma^{n+1}\right)_{\sigma \in \mathcal{F}_\Gamma^i} \right)$ are given by the following *nonconforming-in-time scheme*: for $i = 1, 2$,

$$|K| \frac{u_K^{n+1} - u_K^n}{\tau_i} + \sum_{L \in \mathcal{N}(K)} \tau_{K,L} \left(\varphi_i(u_K^{n+1}) - \varphi_i(u_L^{n+1}) \right) + \sum_{\sigma \in \mathcal{F}_{K,\Gamma}^i} \tau_{K,\sigma} \left(\varphi_i(u_K^{n+1}) - \varphi_i(u_{K,\sigma}^{n+1}) \right) = 0, \quad \forall K \in \mathcal{T}_i, \tag{5.3b}$$

$$
\begin{aligned}
(5.3c)\quad & -\tau_{K,\sigma}\Big(\varphi_i(u_K^{n+1})-\varphi_i(u_{K,\sigma}^{n+1})\Big)+\alpha_{ij,\sigma}\Pi_i(u_{K,\sigma}^{n+1})\\
&=\frac{1}{\tau_i}\int_{J_i^n}\mathcal{P}_{ij}\Big(\tau_{L,\sigma}(\varphi_j(u_L(t))-\varphi_j(u_{L,\sigma}(t)))+\alpha_{ij,\sigma}\Pi_j(u_{L,\sigma}(t))\Big)\,dt,\\
&\qquad\qquad \forall\sigma\in\mathcal{F}_{K,\Gamma}^i,\ \text{and } \sigma=K|L\ (K\in\mathcal{T}_i, L\in\mathcal{T}_j,\ j=3-i),
\end{aligned}
$$

where $\alpha_{ij,\sigma}=\alpha_{ij\,|\sigma}$. The resulting scheme is non-conforming in time. A numerical analysis of this scheme for linear problems has been carried out in [44, 46].

5.2. OSWR-algorithm with nonconforming time discretizations. The solution of the non-conforming in time scheme (5.3) is computed by the following discrete counterpart of the OSWR algorithm: given an initial guess $(\Psi_i^0)_{i=1,2}$ defined on $\Gamma\times(0,T)$, at iteration $k\geq 1$, the initial condition is given by

$$
(5.4a)\qquad u_K^{k,0}=\frac{1}{|K|}\int_K u_0\,\mathrm{d}\mathbf{x},\ \forall K\in\mathcal{T}_i,
$$

and for $n=0,\dots,M_i-1$, the discrete saturations are given by

$$
\begin{aligned}
(5.4b)\quad & |K|\frac{u_K^{k,n+1}-u_K^{k,n}}{\tau_i}+\sum_{L\in\mathcal{N}(K)}\tau_{K,L}\Big(\varphi_i(u_K^{k,n+1})-\varphi_i(u_L^{k,n+1})\Big)\\
&\qquad+\sum_{\sigma\in\mathcal{F}_{K,\Gamma}^i}\tau_{K,\sigma}\Big(\varphi_i(u_K^{k,n+1})-\varphi_i(u_{K,\sigma}^{k,n+1})\Big)=0,\quad \forall K\in\mathcal{T}_i,
\end{aligned}
$$

$$
\begin{aligned}
(5.4c)\quad & -\tau_{K,\sigma}\Big(\varphi_i(u_K^{k,n+1})-\varphi_i(u_{K,\sigma}^{k,n+1})\Big)+\alpha_{ij,\sigma}\Pi_i(u_{K,\sigma}^{k,n+1})=\Psi_{L,\sigma}^{k-1,n+1},\\
&\qquad\qquad \forall\sigma\in\mathcal{F}_{K,\Gamma}^i,\ \text{and } \sigma=K|L\ (K\in\mathcal{T}_i, L\in\mathcal{T}_j,\ j=3-i).
\end{aligned}
$$

Then update the new iterates, for $n=0,\dots,M_i-1$, by

$$
\begin{aligned}
(5.4d)\quad & \Psi_{L,\sigma}^{k,n+1}=\frac{1}{\tau_i}\int_{J_i^n}\mathcal{P}_{ij}\big(\tau_{L,\sigma}(\varphi_j(u_L^{k-1}(t))-\varphi_j(u_{L,\sigma}^{k-1}(t)))+\alpha_{ij,\sigma}\Pi_j(u_{L,\sigma}^{k-1}(t))\big)\,dt,\\
&\qquad\qquad \forall\sigma\in\mathcal{F}_{K,\Gamma}^i,\ \text{and } \sigma=K|L\ (K\in\mathcal{T}_i, L\in\mathcal{T}_j,\ j=3-i).
\end{aligned}
$$

In order to prove that algorithm (5.4) is well defined, one would need to show that Lemma 4.1 can be applied, in order to eliminate the interface unknowns. For this purpose, we suppose that the capillary pressure functions satisfy

$$
(5.5)\qquad \pi_1(0)=\pi_2(0)\ \text{and}\ \pi_1(1)=\pi_2(1).
$$

LEMMA 5.1. *Assume that condition (5.5) holds. Given an element K with a face on the interface $\sigma\in\mathcal{F}_{K,\Gamma}^i$, let $L\subset\Omega_j$ such that $\sigma=K|L$, $j=3-i$. If $\alpha_{ij,\sigma}>\tau_{L,\sigma}$, then there exists a unique $u_{K,\sigma}^{k,n+1}\in[0,1]$ solution of (5.4c), with $\Psi_{L,\sigma}^{k,n+1}$ defined by (5.4d).*

Proof. We first prove that the quantity inside the parenthesis in (5.4d) satisfies the hypotheses of Lemma (4.1). Let

$$
(5.6)\qquad \Phi_{L,\sigma}^{k-1,n+1}=\tau_{L,\sigma}\Big(\varphi_j(u_L^{k-1,n+1})-\varphi_j(u_{L,\sigma}^{k-1,n+1})\Big)+\alpha_{ij,\sigma}\Pi_j(u_{L,\sigma}^{k-1,n+1}),
$$

and define the function $f : (a,b) \longmapsto \tau_{L,\sigma}\varphi_j(a) + \Big(\alpha_{ij,\sigma}\Pi_j(b) - \tau_{L,\sigma}\varphi_j(b)\Big)$, so that $\Phi_{L,\sigma}^{k-1,n+1} = f(u_{L,\sigma}^{k-1,n+1}, u_L^{k-1,n+1})$. It is clear that $(a,b) \in [0,1]^2$, and that f is non-decreasing with respect to a. It remains to study f as a function of b. Because of condition (5.5), the function Π is strictly increasing. We compute

$$\frac{\partial f}{\partial b} = (\alpha_{ij,\sigma} - \tau_{L,\sigma})\lambda(u_{L,\sigma}^{k-1,n+1})\pi_j'(u_{L.\sigma}^{k-1,n+1}),$$

which is positive if $\alpha_{ij,\sigma} > \tau_{L,\sigma}$.

We conclude that the values on the right hand side of (5.4c) also satisfy this inequality, as both the projection $\mathcal{P}_{ij}$ and intergration preserve monotonicity. ∎

COROLLARY 5.1 (Well-posedness of the algorithm). *Assume condition (5.5) holds. Given an initial iterate $(\Psi_i^0)_{i=1,2}$, satisfying Assumption 4.1, and an initial data $u_{\mathcal{T}}^0 \in [0,1]$, the nonconforming-in-time scheme (5.4) admits a unique solution $u_{\mathcal{D}}^k$ that satisfies, $\forall 1 \le i \le I$, for all $K \in \mathcal{T}_i$, for all $n \in \{1,...,M_i\}$:*

$$0 \le u_K^{k,n} \le 1. \tag{5.7}$$

Proof. The proof is by induction on k, the base case being given by the initial condition, and the induction step follows from Lemma 5.1 and an analysis similar to that carried out in the proof of Proposition 4.2 ∎

REMARK 5.1. *For problems with long time computations, one can split the time interval into time windows, in which a few iterations of the above OSWR algorithm are performed by the discontinuous Galerkin method in time, with nonconforming projection between space-time grids on the interfaces. Time windows are used in order to reduce the number of iterations of the algorithm as shown in [45] for linear heterogeneous problems, and in Section 6 for the two-phase flow problem.*

5.3. Particular case of conforming time discretizations. In this section, the time grids are assumed to be conforming, and we set $\mathcal{M} := \mathcal{M}_1 = \mathcal{M}_2$, and $M := M_1 = M_2$. Then, using the notation (5.2), the transmission conditions (5.4c)–(5.4d) reduces to the more usual form: for $i = 1, 2$, $j = 3 - i$,

$$\begin{aligned} &-\tau_{K,\sigma}(\varphi_i(u_K^{n+1}) - \varphi_i(u_{K,\sigma}^{n+1})) + \alpha_{ij,\sigma}\Pi_i(u_{K,\sigma}^{n+1}) = \\ &\qquad -\tau_{L,\sigma}(\varphi_j(u_L^{n+1}) - \varphi_j(u_{L,\sigma}^{n+1})) + \alpha_{ij,\sigma}\Pi_j(u_{L,\sigma}^{n+1}). \end{aligned} \tag{5.8}$$

DEFINITION 5.2. *Let $\mathcal{D}$ be an admissible discretization of $\Omega\times(0,T)$ in the sense of the Definition 5.1. We define $\mathcal{Y}(\mathcal{D})$ the space of the functions $u_{\mathcal{D}}$ whose restriction on $\overline{\Omega}_i \times (0,T)$ belongs to $\mathcal{X}(\mathcal{D}_i)$ (see Definition 4.2). We define the solution $u_{\mathcal{D}} \in \mathcal{Y}(\mathcal{D})$ of the scheme (5.3) by*

$$u_{\mathcal{D}}(\mathbf{x},t) = u_K^n \quad \text{if } (\mathbf{x},t) \in K \times J^n,\ K \in \mathcal{T},\ \text{and } J^n \in \mathcal{M}, \tag{5.9}$$

and for $\mathbf{x} \in \sigma = K|L$ for $K \in \mathcal{T}_1$, $L \in \mathcal{T}_2$, for $t \in J^n$, the traces

$$u_{\mathcal{D}}|_\Gamma(\mathbf{x},t) = u_{K,\sigma}^n, \quad \text{and} \quad u_{\mathcal{D}}|_{\Gamma_{rl}}(\mathbf{x},t) = u_{L,\sigma}^n. \tag{5.10}$$

From (5.8), we have the following result

LEMMA 5.2. *Let $\mathcal{D}$ be an admissible discretization of $\Omega \times (0,T)$ in the sense of the Definition 5.1. Then, the scheme (5.3) with Robin transmission conditions is*

equivalent to scheme given by (5.3a)–(5.3b) together with the following natural transmission conditions on $\Gamma \times (0,T)$*:* $\forall \sigma \in \mathcal{F}_\Gamma$*, and* $\sigma = K|L$*, for* $K \in \mathcal{T}_1$*,* $L \in \mathcal{T}_2$*, for all* $n \in \{0, \dots, M-1\}$*,*

$$-\tau_{K,\sigma}\Big(\varphi_1(u_K^{n+1}) - \varphi_1(u_{K,\sigma}^{n+1})\Big) = \tau_{L,\sigma}\Big(\varphi_2(u_L^{n+1}) - \varphi_2(u_{L,\sigma}^{n+1})\Big), \tag{5.11}$$

$$\Pi_1(u_{K,\sigma}^{n+1}) = \Pi_2(u_{L,\sigma}^{n+1}). \tag{5.12}$$

Then, the analysis in [22, 31] together with Lemma 5.2 lead to the following result:

COROLLARY 5.2. *Assume that Assumptions 2.1 and 4.1 hold. Let* $(\mathcal{D}_m)_m$ *be a sequence of admissible discretizations of* $\Omega \times (0,T)$*; then, for all* $m \in \mathbb{N}$*, there exists a discrete solution* $u_{\mathcal{D}_m} \in \mathcal{Y}(\mathcal{D}_m)$ *to the scheme (5.3). Moreover, if* $\lim_{m\to\infty} \mathrm{size}(\mathcal{D}_m) = 0$*, and if there exists* $\zeta > 0$ *such that* $\mathrm{reg}(\mathcal{D}_m) \le \zeta$*, then,* $\exists u \in L^p(\Omega \times (0,T))$*, such that (up to a subsequence)*

$$u_{\mathcal{D}_m} \to u \in L^p(\Omega \times (0,T)), \quad \forall p \in [1,\infty), \tag{5.13}$$

where u *is a weak solution to the multidomain problem (2.9)–(3.1) in the sense of Definition 2.1.*

6. Numerical results. We now study the numerical behavior of the Optimized Schwarz waveform relaxation algorithm.

6.1. Example 1: Validation experiment with two rock types. Let us consider a domain $\Omega = [0,1]^3$ decomposed into two subdomains with two rock types (see top left image on Figure 6.1). The mobilities are given by

$$\lambda_{o,i}(u) = u, \quad \text{and} \quad \lambda_{g,i}(u) = (1-u),\ i \in \{1,2\},$$

and the capillary pressure curves are given by

$$\pi_1(u) = 5u^2, \quad \text{and} \quad \pi_2(u) = 5u^2 + 1.$$

For the initial condition, we suppose that the domain contains some quantity of gas, situated only within Ω_1, i.e.

$$u_0 = \begin{cases} 0.9 & \text{if } x < 0.4, \\ 0 & \text{otherwise.} \end{cases}$$

For the spatial discretization, we use a uniform rectangular mesh with $20 \times 20 \times 20$ elements. For the time discretization, we use nonconforming time grids, constant in each subdomain, with $\delta t_1 = 10^{-3}$, and $\delta t_2 = \frac{1}{8}10^{-2}$.

The evolution of the saturation at four time steps is shown in Figure 6.1. We remark that at the beginning of the simulation, approximately until $t \approx 0.02$, the gas cannot penetrate to the domain Ω_2, since the capillary pressure is lower than the threshold value $\pi_2(0) = 1$, which is known as the entry pressure (see Figure 2.1). The saturation of the trapped gas in Ω_1 as well as the capillary pressure increase until the capillary pressure reaches the entry pressure. This is physically the phenomenon of capillary trapping that model (2.1) describes and which is mathematically due to the degenerate (vanishing) diffusion: indeed, if diffusion was non-vanishing, the gas saturation would be non-zero in the subdomain Ω_2 from the very beginning, and not only after the barrier brake (in contrast to what can be observed in Figure Figure 6.1).

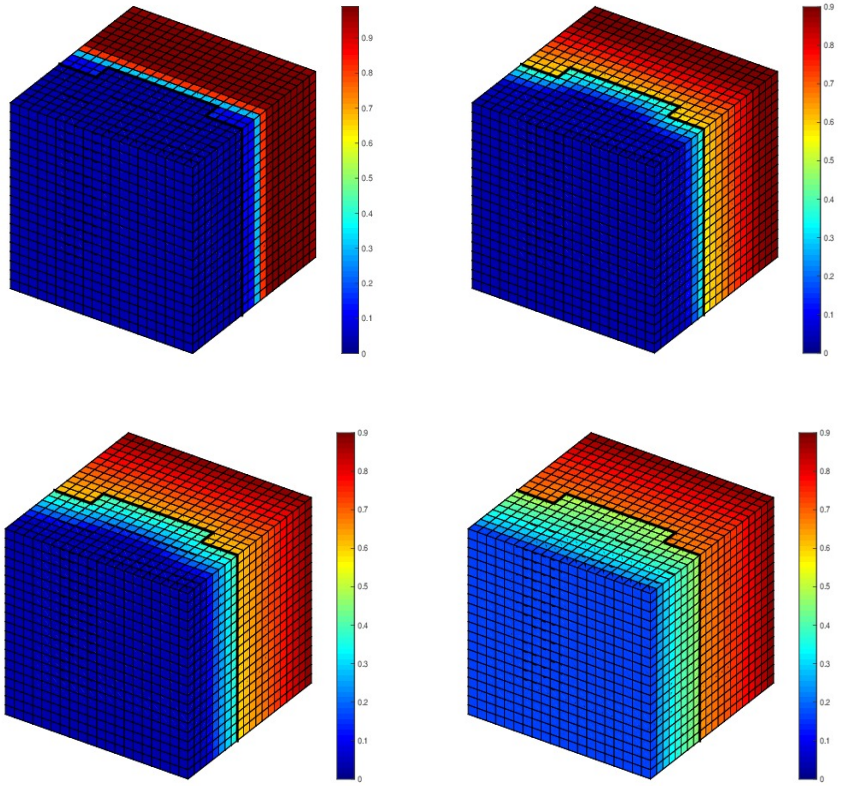

FIG. 6.1. *Example 1: saturation $u(t)$, for t=0.019, t=0.3,, t=0.6, and t=3*

Figure 6.2 shows the evolution of the capillary pressure at four time steps. Figure 6.3 (top) shows evolution of the saturation, the capillary pressure and the diffusion function φ, along a line orthogonal to the interface Γ. We see that the capillary pressure becomes continuous when the entry pressure is reached, and the domain Ω_2 is infiltrated whereas the discontinuity of the saturation and the function φ persists at the interface between the two rocks.

We now analyze the efficiency in time of the method with nonconforming time steps. We compute a reference solution as the converged multidomain solution with conforming fine time grids $\delta t_f = \frac{1}{4}10^{-3}$, and where the relative residual is taken smaller than 10^{-12}. We then compare the solution obtained with the nonconforming time steps, as described above with two solutions computed first with conforming fine time steps ($\delta t_1 = \delta t_2 = 10^{-3}$) and then with conforming coarse time steps (($\delta t_1 = \delta t_2 = \frac{1}{8}10^{-2}$)). Figure 6.4 (bottom) shows the error in the saturation along a line orthogoanl to the interface at three different time steps. One can see that the nonconforming solution as well as the solution with conforming and fine steps are in close agreement with the reference solution, whereas the solution with coarse time steps has a larger error. This confirms that nonconforming time grids with respect to the rock type preserve the accuracy in time of the multidomain solution.

Finally, we study the convergence behavior of the optimized Schwarz waveform

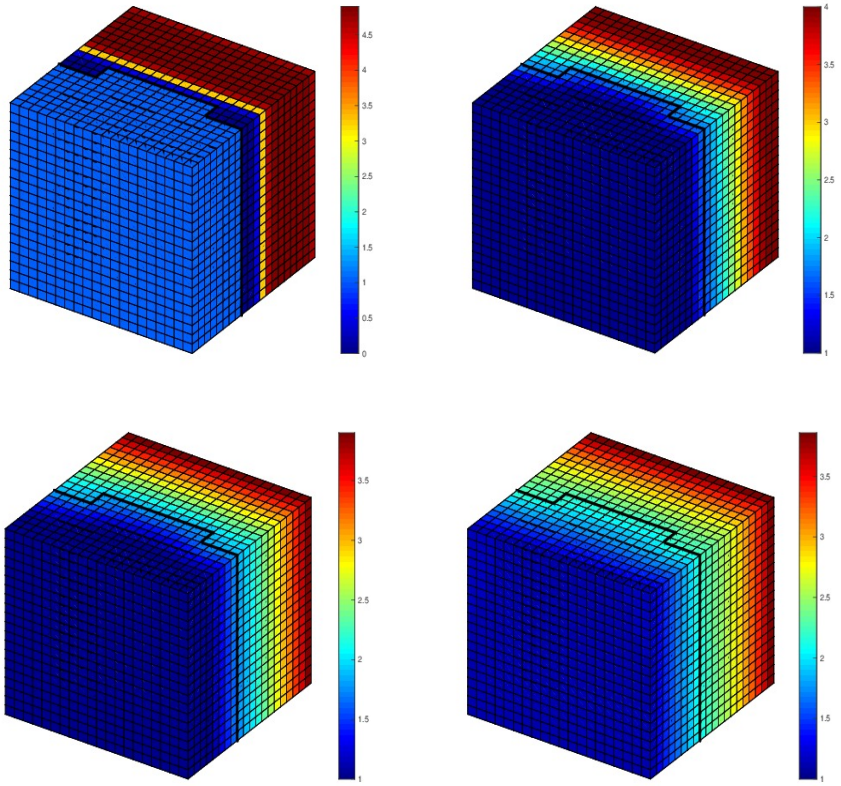

FIG. 6.2. *Example 1: Capillary pressure $\pi(u(t))$, for t=0.019, t=0.3,, t=0.6, and t=3*

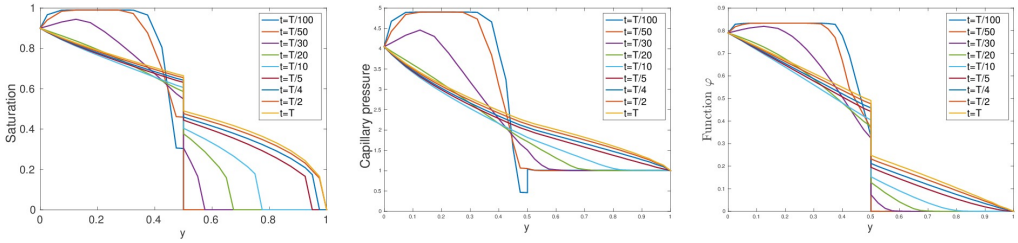

FIG. 6.3. *Example 1. From left to right: evolution of the saturation, capillary pressure and diffusion function along a line orthogonal to the interface.*

relaxation (OSWR) algorithm. We use as solver for the nonlinear subdomain problems a Newton's method where the tolerance is fixed to 10^{-8}. The tolerance of the OSWR algorithm is 10^{-6}. The Robin parameters are chosen following the approach described in Section 3.2. We show in Figure 6.5 (right) the relative residuals comparing the convergence history with the parameters calculated numerically by minimizing the convergence factor for the linearized problem and that of with the best parameters located in the zone giving the smaller errors after the same number of iterations (see Figure 6.5 left). We can show that the values obtained by this approach may not be

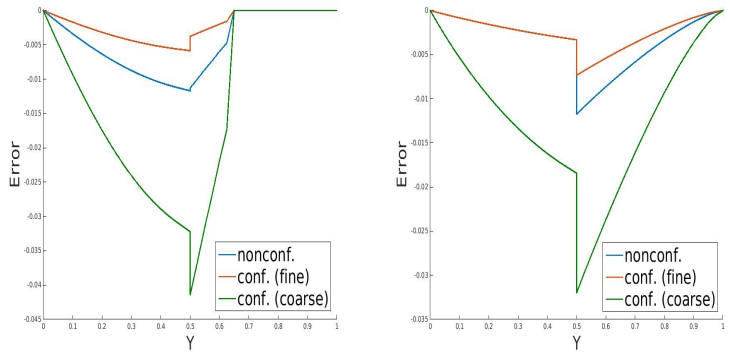

FIG. 6.4. *Example 1. Error in saturation along a line orthogonal to the interface, nonconforming and conforming (coarse and fine) time-steps. Left $T = T_f/20$, right, $T = T_f$.*

the best but still lead to a fast enough convergence. Moreover, the convergence may be improved and the parameters can be nearly optimal if one consider time windows, as shown in the last example.

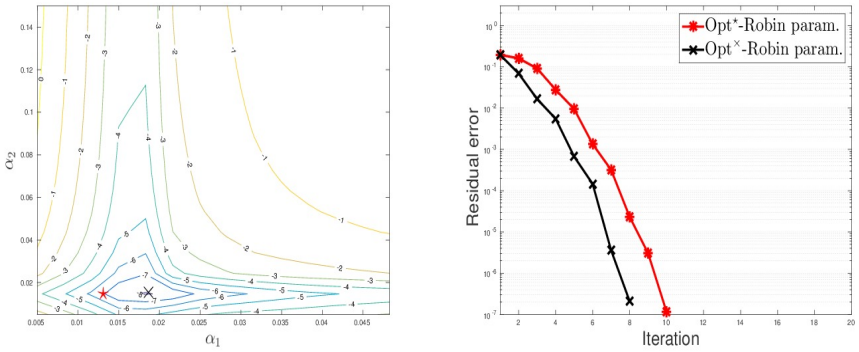

FIG. 6.5. *Example 1: Left: Level curves for the residual error obtained after 10 iterations for various values of the parameters α_1 and α_2. The star (in red) marked the parameters obtained with the minimization process of the convergence factor applied to the linearized problem which is close to the best one marked by times symbol (in black). Right: The convergence curves.*

6.2. Example 2: DNAPL infiltration. In this example, we consider a three-dimensional DNAPL infiltration problem with two different rock types. The medium contains a lens with different capillary pressure and relative permeability curves. The gas and water mobilities are given by

$$\lambda_{o,i}(u) = u^2, \quad \text{and} \quad \lambda_{g,i}(u) = 3(1-u)^2,\ i \in \{1,2\},$$

and the capillary pressure curves have the form

$$\pi_1(u) = \ln(1-u), \quad \text{and} \quad \pi_2(u) = 0.5 - \ln(1-u).$$

The capillary pressure curves in that case are more complicate as $\pi_1(u) \to -\infty$ $\pi_2(u) \to +\infty$ if $u \to 1$. The gas is injected along one side of the domain and a

Dirichlet condition is imposed on the opposite face, while no-flow boundary conditions are imposed on the remaining faces.

We use a uniform mesh with 17576 elements (corresponding to 26 elements in each layer of each direction), and nonconforming time steps with $\delta t_1 = 1/2$, and $\delta t_2 = 1/3$ for $t \in [0, 500]$. The geometry and the spatial discretization are shown in Figure 6.6.

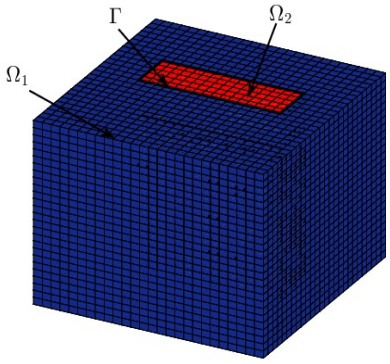

FIG. 6.6. *Example 2: The geometry and the mesh*

Figure 6.7 shows the evolution of the saturation over the whole domain, while Figure 6.8 shows the saturation on the slice at the middle of the domain Ω in the z-direction (using the same color scale). In this experiment, the flow is driven not only by buoyancy, but also by the difference in the capillary pressures. In contrast to the previous example, when the gas reaches the interface, the flow crosses immediately the interface through the domain Ω_2 and the saturation front snakes along the interface. The gas accumulates into the lens until it eventually spreads into the surrounding medium. The lens acts as a capillary trap (see also [32] or [18]): it is much easier for the gas to enter the lens than to leave it, because of the difference in capillary pressures.

The Robin parameters are again calculated using the procedure of Section 3.2. Here, we also compare the optimized Schwarz method with only one optimized parameter for both subdomains (one-sided method) and that with two different optimized parameters (two-sided method). In Figure 6.9 (right), we compare the convergence for both methods. Clearly the two-sided method improves the convergence speed compared to the one-sided method. The two-sided OSWR method needs only 8 iterations to reach a residual error of 10^{-6} compared to the one-sided, which needs 12 iterations.

6.3. Example 3: An example of multidomain solution with time windows for three rock types. Our final example has three rock types as depicted in Figure 6.10 (left). We use a uniform mesh with 8000 elements, and nonconforming time steps. The mobilities used in this example are the same as in the first example and the capillary pressure curves are given by

$$\pi_1(u) = 3u^2, \quad \pi_2(u) = 5u^2, \text{ and } \quad \pi_3(u) = 3u^2 + 0.5.$$

This numerical experiment shows not only the ability of the method to satisfy the interface conditions between the different rock types, but also the ability of handling different boundary conditions. Dirichlet boundary conditions are imposed on the

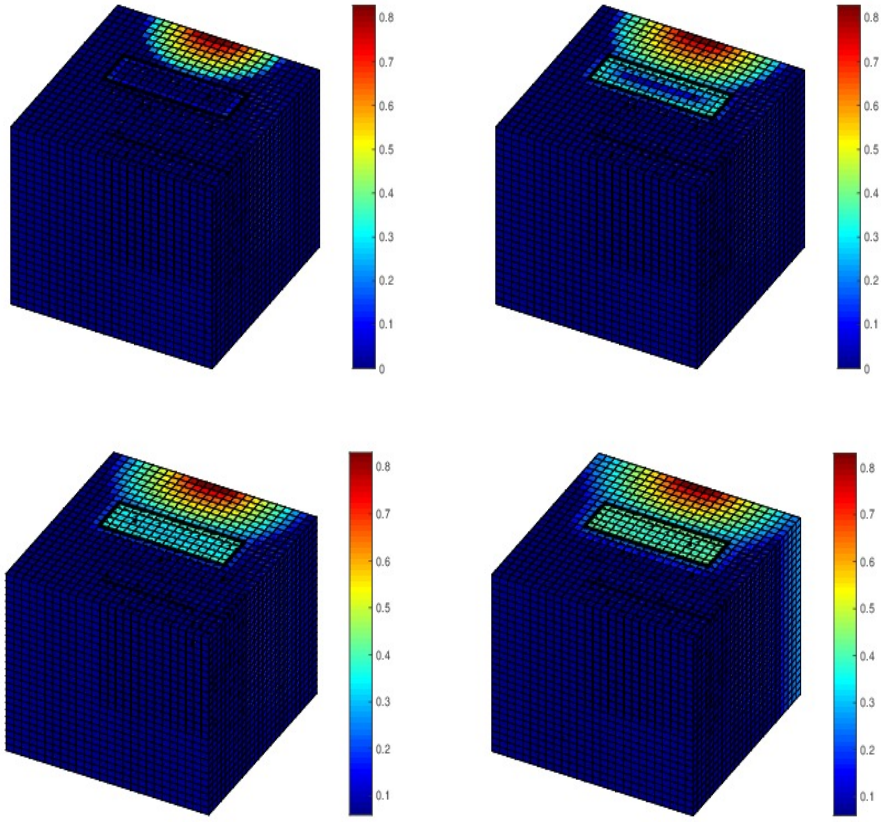

FIG. 6.7. *Example 2: Saturation $u(t)$, for t=100, t=200, t=350, t=480*

inflow and outflow boundaries. The inflow boundary, given by $\Gamma_{in} = \{x = 0\} \times \{z > 0.5\}$ has $s = 0.9$. On the outflow boundary $\Gamma_{out} = \{x = 1\}$, the saturation at time t^{n+1} is set equal to that inside the closest cell at time t^n (see [2]).

The space domain is split into 7 subdomains that respect to the rock type (see Figure 6.11). The time interval $[0, 2500]$ is decomposed into 10 equal time windows. The spatial grids on the interface are conforming but the time steps are different in the time windows. The OSWR algorithm is employed over one time window at a time, and only after convergence on the current time window is the next time window treated by the algorithm. The OSWR method needs 32 iterations overall to converge, with 5 iterations for the first time window, and then 3 iterations for the remaining ones. We have observed that the use of time windows leads to a significantly better estimate of the Robin parameters, and the iteration number is now much closer to the best possible in the algorithm.

Figure 6.11 shows the saturation in the whole domain at four time steps, Figure 6.12 shows the saturation at the bottom face of Ω using the same color scale, and Figure 6.10 (right) shows the velocity streamlines in the whole domain. One can see that most of the gas flows through the subdomains Ω_1 that has the lowest capillary pressure curve. The gas only enters the other subdomains once the capillary pressure

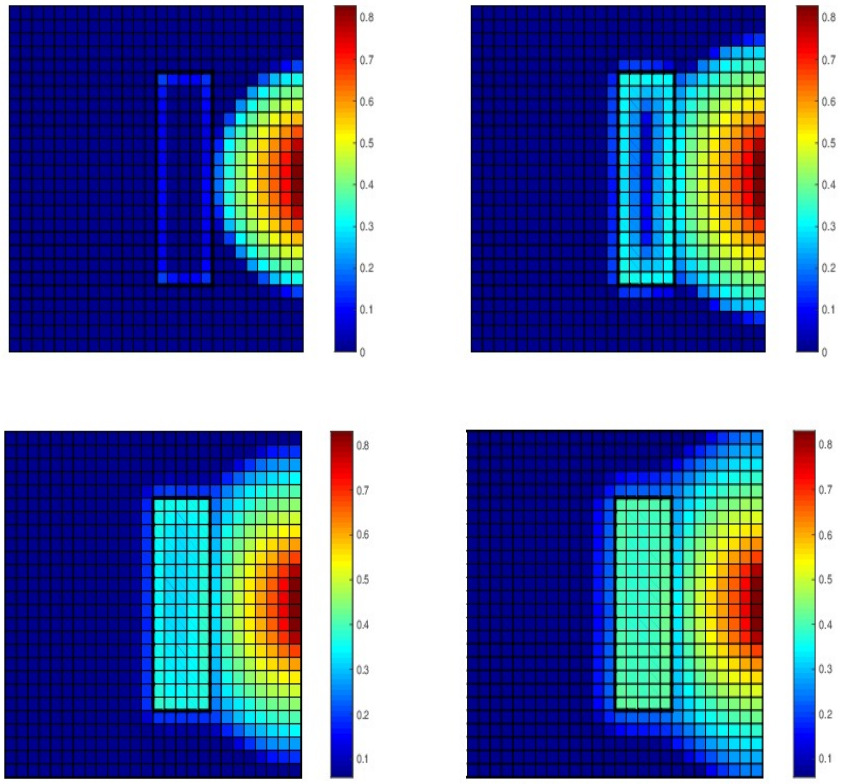

FIG. 6.8. *Example 2: Saturation $u(t)$ on a slice at the middle of the domain Ω in the z-direction, for t=100, t=200, t=350, t=480*

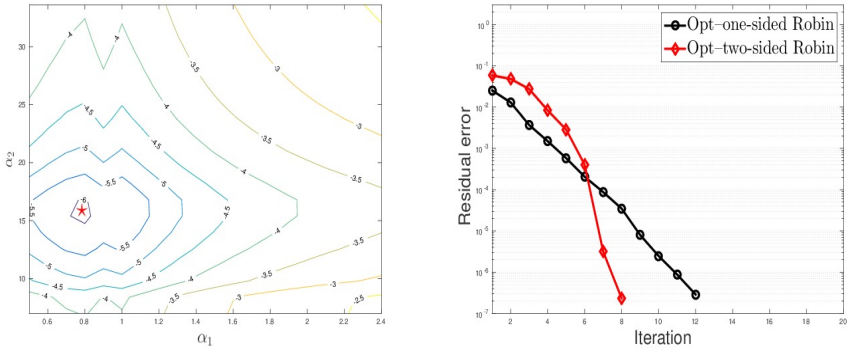

FIG. 6.9. *Example 2: Left: Level curves for the residual error obtained after 8 iterations for various values of the parameters α_1 and α_2. The red star shows the optimized parameters. Right: The convergence curves of the optimized Schwarz method with one-sided optimized Robin conditions and two-sided optimized Robin conditions.*

reaches the entry pressure for the respective rock.

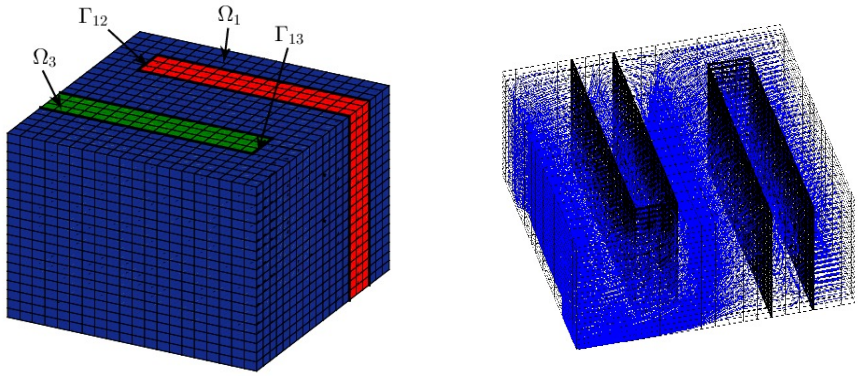

FIG. 6.10. *Example 3: Left: The geometry and the mesh. Right: Velocity streamlines.*

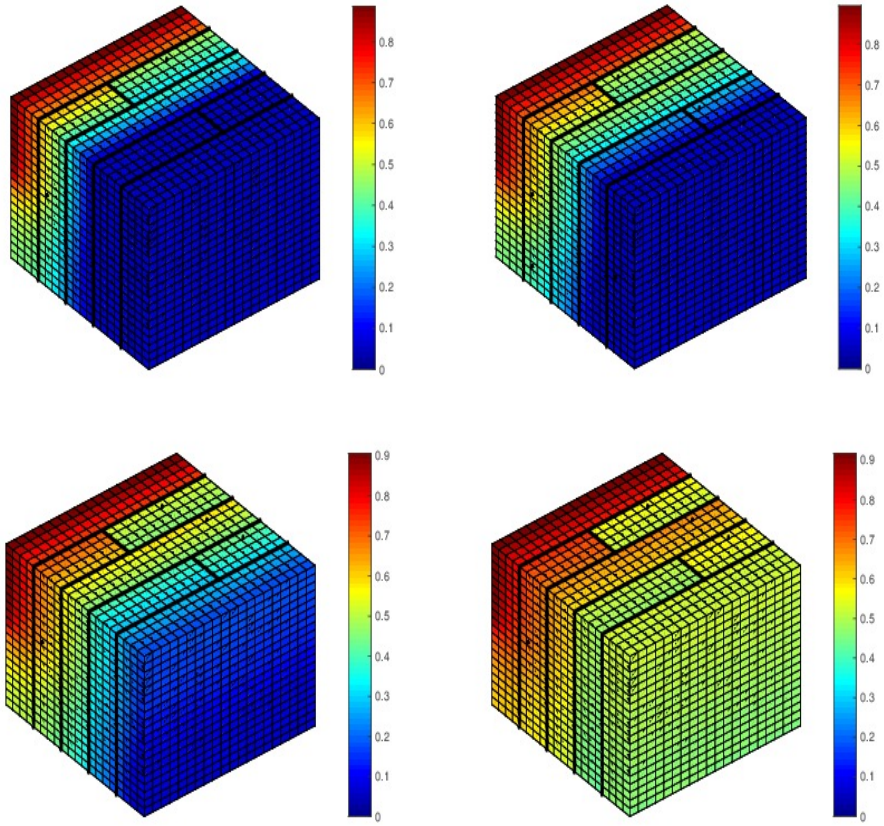

FIG. 6.11. *Example 3: Saturation $u(t)$, for t=500, t=1000, t=2000 and t=4000*

7. Conclusion. This paper combines an Optimized Schwarz Waveform Relaxation method with a finite volume scheme for the discretization of two-phase flows in a

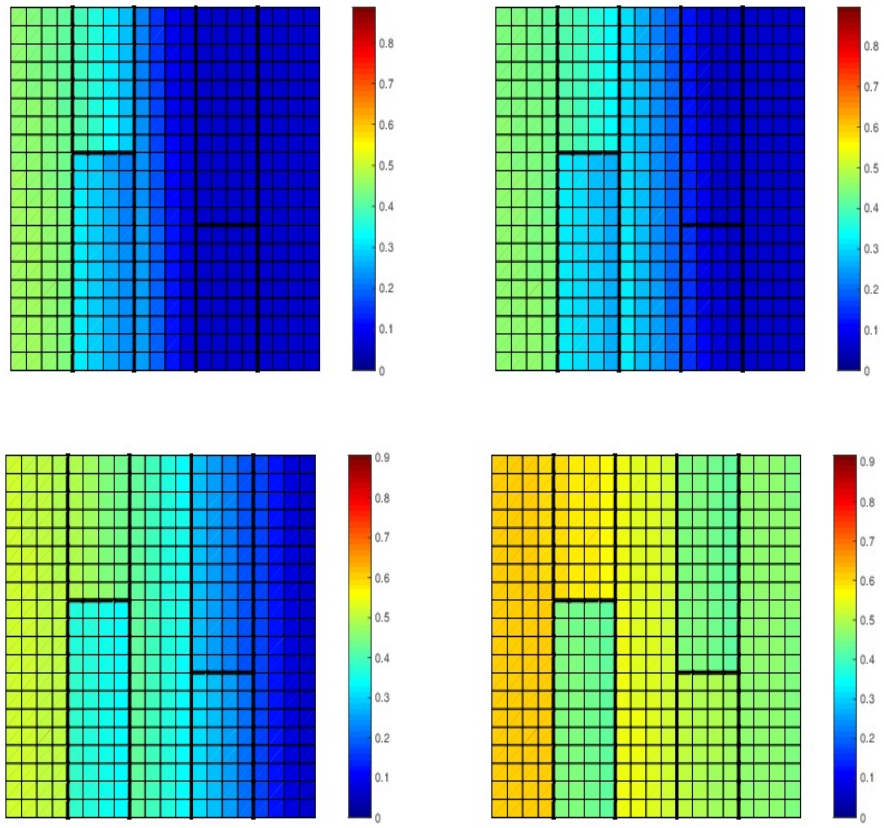

FIG. 6.12. *Example 3: Saturation $u(t)$ at the bottom face of Ω, for t=500, t=1000, t=2000 and t=4000*

porous medium made up of different rock types. The model problem we consider only takes into account the diffusive effects for the saturation, and deals with discontinuous capillary pressure curves at the interface between the rocks. An existence result for the subdomain two-phase flow problem with nonlinear Robin boundary condition is presented.

The OSWR algorithm provides a natural way to treat the discontinuity of the saturation between rock types. The method allows for different time steps in the subdomains, so as to adapt to the time scales imposed by the different capillary pressure curves. A discontinuous Galerkin method in time is used, with projection between the space–time grids on the interfaces to match the local solutions. The convergence of the scheme is improved through the use of time windows. Several numerical results highlight the efficiency of the proposed method, and confirm that the nonlinear interface conditions, which are enforced in the context of a OSWR-algorithm, are captured in a robust and accurate way.

REFERENCES

[1] Elyes Ahmed, Sarah Ali Hassan, Caroline Japhet, Michel Kern, and Martin Vohralík, *A posteriori error estimates and stopping criteria for space-time domain decomposition for two-phase flow between different rock types*. Working paper or preprint, June 2017.

[2] Elyes Ahmed, Jérôme Jaffré, and Jean E. Roberts, *A reduced fracture model for two-phase flow with different rock types*, Math. Comput. Simulation, 137 (2017), pp. 49–70.

[3] Ahmed Ait Hammou Oulhaj, *Numerical analysis of a finite volume scheme for a seawater intrusion model with cross-diffusion in an unconfined aquifer*, Numerical Methods for Partial Differential Equations, 34 (2018), pp. 857–880.

[4] Ait Hammou Oulhaj, Ahmed, Cancès, Clément, and Chainais-Hillairet, Claire, *Numerical analysis of a nonlinearly stable and positive control volume finite element scheme for richards equation with anisotropy*, ESAIM: M2AN, 52 (2018), pp. 1533–1567.

[5] Sarah Ali Hassan, Caroline Japhet, Michel Kern, and Martin Vohralík, *A posteriori stopping criteria for optimized Schwarz domain decomposition algorithms in mixed formulations*, Comput. Methods Appl. Math., 18 (2018), pp. 495–519.

[6] Sarah Ali Hassan, Caroline Japhet, and Martin Vohralík, *A posteriori stopping criteria for space-time domain decomposition for the heat equation in mixed formulations*, Electron. Trans. Numer. Anal., 49 (2018), pp. 151–181.

[7] Brahim Amaziane, S Antontsev, Leonid Pankratov, and Andrey Piatnitski, *Homogenization of immiscible compressible two-phase flow in porous media: application to gas migration in a nuclear waste repository*, Multiscale Modeling & Simulation, 8 (2010), pp. 2023–2047.

[8] B Amaziane, A Bourgeat, and H El Amri, *Existence of solutions to various rock types odel model of two-phase flow in porous media*, Applicable Analysis, 60 (1996), pp. 121–132.

[9] Brahim Amaziane, Mustapha El Ossmani, and Mladen Jurak, *Numerical simulation of gas migration through engineered and geological barriers for a deep repository for radioactive waste*, Computing and Visualization in Science, 15 (2012), pp. 3–20.

[10] L. Ambrosio and G. Dal Maso, *A general chain rule for distributional derivatives*, Proc. Amer. Math. Soc., 108 (1990), pp. 691–702.

[11] Boris Andreianov, Konstantin Brenner, and Clément Cancès, *Approximating the vanishing capillarity limit of two-phase flow in multi-dimensional heterogeneous porous medium*, ZAMM Z. Angew. Math. Mech., 94 (2014), pp. 655–667.

[12] Boris Andreianov, Clément Cancès, and Ayman Moussa, *A nonlinear time compactness result and applications to discretization of degenerate parabolic-elliptic PDEs*, J. Funct. Anal., 273 (2017), pp. 3633–3670.

[13] Boris Andreianov and Mohamed Karimou Gazibo, *Entropy formulation of degenerate parabolic equation with zero-flux boundary condition*, Zeitschrift für angewandte Mathematik und Physik, 64 (2013), pp. 1471–1491.

[14] K. Aziz and A. Settari, *Petroleum reservoir simulation*, Applied Science Publishers, 1979.

[15] D. Bennequin, M. J. Gander, and L. Halpern, *A homographic best approximation problem with application to optimized Schwarz waveform relaxation*, Math. Comp., 78 (2009), pp. 185–223.

[16] Heiko Berninger, Sébastien Loisel, and Oliver Sander, *The 2-Lagrange multiplier method applied to nonlinear transmission problems for the Richards equation in heterogeneous soil with cross points*, SIAM J. Sci. Comput., 36 (2014), pp. A2166–A2198.

[17] Paul-Marie Berthe, Caroline Japhet, and Pascal Omnes, *Space-Time Domain Decomposition with Finite Volumes for Porous Media Applications*, in Domain Decomposition Methods in Science and Engineering XXI, J. Erhel, M.J. Gander, L. Halpern, G. Pichot, T. Sassi, and O. Widlund, eds., vol. 98 of Lecture Notes in Computational Science and Engineering, 2014, pp. 483–490.

[18] Michiel Bertsch, R Dal Passo, and CJ Van Duijn, *Analysis of oil trapping in porous media flow*, SIAM Journal on Mathematical Analysis, 35 (2003), pp. 245–267.

[19] Alain Bourgeat and Mladen Jurak, *A two level scaling-up method for multiphase flow in porous media; numerical validation and comparison with other methods*, Computational geosciences, 14 (2010), pp. 1–14.

[20] Konstantin Brenner, Clément Cancès, and Danielle Hilhorst, *Finite volume approximation for an immiscible two-phase flow in porous media with discontinuous capillary pressure*, Computational Geosciences, 17 (2013), pp. 573–597.

[21] Filipa Caetano, Martin J Gander, Laurence Halpern, Jérémie Szeftel, et al., *Schwarz waveform relaxation algorithms for semilinear reaction-diffusion equations.*, NHM, 5 (2010), pp. 487–505.

[22] Clément Cancès, *Nonlinear parabolic equations with spatial discontinuities*, NoDEA Nonlinear Differential Equations Appl., 15 (2008), pp. 427–456.

[23] ———, *Finite volume scheme for two-phase flows in heterogeneous porous media involving capillary pressure discontinuities*, M2AN Math. Model. Numer. Anal., 43 (2009), pp. 973–1001.

[24] Clément Cances, *On the effects of discontinuous capillarities for immiscible two-phase flows in porous media made of several rock-types.*, NHM, 5 (2010), pp. 635–647.

[25] Clément Cancès, Thierry Gallouët, and Alessio Porretta, *Two-phase flows involving capillary barriers in heterogeneous porous media*, Interfaces Free Bound., 11 (2009), pp. 239–258.

[26] Clément Cancès, Iuliu Sorin Pop, and Martin Vohralík, *An a posteriori error estimate for vertex-centered finite volume discretizations of immiscible incompressible two-phase flow*, Math. Comp., 83 (2014), pp. 153–188.

[27] Guy Chavent and Jérôme Jaffré, *Mathematical models and finite elements for reservoir simulation: single phase, multiphase and multicomponent flows through porous media*, Elsevier, 1986.

[28] Philippe G. Ciarlet, *Linear and Nonlinear Functional Analysis with Applications*, SIAM, 2013.

[29] Daniele A. Di Pietro, Eric Flauraud, Martin Vohralík, and Soleiman Yousef, *A posteriori error estimates, stopping criteria, and adaptivity for multiphase compositional Darcy flows in porous media*, J. Comput. Phys., 276 (2014), pp. 163–187.

[30] Victorita Dolean, Pierre Jolivet, and Frédéric Nataf, *An introduction to domain decomposition methods*, Society for Industrial and Applied Mathematics (SIAM), Philadelphia, PA, 2015. Algorithms, theory, and parallel implementation.

[31] Guillaume Enchéry, R. Eymard, and A. Michel, *Numerical approximation of a two-phase flow problem in a porous medium with discontinuous capillary forces*, SIAM J. Numer. Anal., 43 (2006), pp. 2402–2422.

[32] Alexandre Ern, Igor Mozolevski, and Luciane Schuh, *Discontinuous Galerkin approximation of two-phase flows in heterogeneous porous media with discontinuous capillary pressures*, Computer methods in applied mechanics and engineering, 199 (2010), pp. 1491–1501.

[33] Robert Eymard, Thierry Gallouët, and Raphaèle Herbin, *Finite volume methods*, in Handbook of numerical analysis, Ph. G. Ciarlet and J.-L. Lions, eds., vol. 7, Elsevier, 2000, pp. 713–1018.

[34] Robert Eymard, Thierry Gallouët, Danielle Hilhorst, and Y Naït Slimane, *Finite volumes and nonlinear diffusion equations*, RAIRO-Modélisation mathématique et analyse numérique, 32 (1998), pp. 747–761.

[35] Martin J. Gander, *Optimized Schwarz methods*, SIAM J. Numer. Anal., 44 (2006), pp. 699–731 (electronic).

[36] M. J. Gander and L. Halpern, *Optimized Schwarz waveform relaxation methods for advection reaction diffusion problems*, SIAM J. Numer. Anal., 45 (2007), pp. 666–697.

[37] M. J. Gander, L. Halpern, and F. Nataf, *Optimal Schwarz waveform relaxation for the one dimensional wave equation*, SIAM J. Numer. Anal., 41 (2003), pp. 1643–1681.

[38] Martin J. Gander and Caroline Japhet, *Algorithm 932: PANG: software for nonmatching grid projections in 2D and 3D with linear complexity*, ACM Trans. Math. Software, 40 (2013), pp. Art. 6, 25.

[39] Martin J. Gander, Caroline Japhet, Yvon Maday, and Frédéric Nataf, *A New Cement to Glue Nonconforming Grids with Robin Interface Conditions: The Finite Element Case*, in Domain Decomposition Methods in Science and Engineering, T. J. Barth, M. Griebel, D. E. Keyes, R. M. Nieminen, D. Roose, T. Schlick, R. Kornhuber, R. Hoppe, J. Périaux, O. Pironneau, O. Widlund, and J. Xu, eds., Berlin, Heidelberg, 2005, Springer Berlin Heidelberg, pp. 259–266.

[40] Benjamin Ganis, Kundan Kumar, Gergina Pencheva, Mary F. Wheeler, and Ivan Yotov, *A global Jacobian method for mortar discretizations of a fully implicit two-phase flow model*, Multiscale Model. Simul., 12 (2014), pp. 1401–1423.

[41] Florian Haeberlein, Laurence Halpern, and Anthony Michel, *Newton-Schwarz optimised waveform relaxation Krylov accelerators for nonlinear reactive transport*, in Domain decomposition methods in science and engineering XX, vol. 91 of Lect. Notes Comput. Sci. Eng., Springer, Heidelberg, 2013, pp. 387–394.

[42] ———, *Schwarz Waveform Relaxation and Krylov Accelerators for Reactive Transport.* working paper or preprint, Aug. 2015.

[43] Laurence Halpern and Florence Hubert, *A finite volume Ventcell-Schwarz algorithm for advection-diffusion equations*, SIAM Journal on Numerical Analysis, 52 (2014), pp. 1269–1291.

[44] Laurence Halpern, Caroline Japhet, and Jérémie Szeftel, *Discontinuous Galerkin and nonconforming in time optimized Schwarz waveform relaxation*, in Domain decomposition methods in science and engineering XIX, Springer, 2011, pp. 133–140.

[45] ———, *Optimized Schwarz waveform relaxation and discontinuous Galerkin time stepping for heterogeneous problems*, SIAM J. Numer. Anal., 50 (2012), pp. 2588–2611.

[46] Thao-Phuong Hoang, Jérôme Jaffré, Caroline Japhet, Michel Kern, and Jean E Roberts, *Space-time domain decomposition methods for diffusion problems in mixed formulations*, SIAM Journal on Numerical Analysis, 51 (2013), pp. 3532–3559.

[47] Thao-Phuong Hoang, Caroline Japhet, Michel Kern, and Jean E Roberts, *Space-time domain decomposition for advection-diffusion problems in mixed formulations*, Mathematics and Computers in SImulation, (2016). to appear.

[48] T. T. P. Hoang, C. Japhet, M. Kern, and J. E Roberts, *Ventcell conditions with mixed formulations for flow in porous media*, in Decomposition Methods in Science and Engineering XXII, T. Dickopf, M.J. Gander, L. Halpern, R. Krause, and L. F. Pavarino, eds., vol. 104 of Lecture Notes in Computational Science and Engineering, Springer, 2016, pp. 531–540.

[49] C. Japhet and Frédéric Nataf, *The best interface conditions for domain decomposition methods: absorbing boundary conditions*, in Absorbing Boundaries and Layers, Domain Decomposition Methods, Nova Sci. Publ., Huntington, NY, 2001, pp. 348–373.

[50] Florian Lemarié, Laurent Debreu, and Eric Blayo, *Toward an optimized global-in-time schwarz algorithm for diffusion equations with discontinuous and spatially variable coefficients, part 1: the constant coefficients case*, Electron. Trans. Numer. Anal, 40 (2013), pp. 148–169.

[51] V. Martin, *An optimized Schwarz waveform relaxation method for the unsteady convection diffusion equation in two dimensions*, Appl. Numer. Math., 52 (2005), pp. 401–428.

[52] Igor Mozolevski and Luciane Schuh, *Numerical simulation of two-phase immiscible incompressible flows in heterogeneous porous media with capillary barriers*, Journal of Computational and Applied Mathematics, 242 (2013), pp. 12–27.

[53] J. M. Ortega and W. C. Rheinboldt, *Iterative Solution of Nonlinear Equations in Several Variables*, Computer Science and Applied Mathematics, Academic Press, 1970.

[54] Kévin Santugini, *A Discontinuous Coarse Space (DCS) Algorithm for Cell Centered Finite Volume Based Domain Decomposition Methods: The DCS-RJMin Algorithm*, in Domain Decomposition Methods in Science and Engineering XXII, Springer, 2016, pp. 379–387.

[55] Jan Ole Skogestad, Eirik Keilegavlen, and Jan M. Nordbotten, *Domain decomposition strategies for nonlinear flow problems in porous media*, J. Comput. Phys., 234 (2013), pp. 439–451.

[56] ———, *Two-scale preconditioning for two-phase nonlinear flows in porous media*, Transp. Porous Media, 114 (2016), pp. 485–503.

[57] C. J. Van Duijn, J. Molenaar, and M. J. De Neef, *The effect of capillary forces on immiscible two-phase flow in heterogeneous porous media*, Transport in Porous Media, 21 (1995), pp. 71–93.

[58] Martin Vohralík and Mary F. Wheeler, *A posteriori error estimates, stopping criteria, and adaptivity for two-phase flows*, Comput. Geosci., 17 (2013), pp. 789–812.

[59] I. Yotov, *A mixed finite element discretization on non-matching multiblock grids for a degenerate parabolic equation arising in porous media flow*, East-West J. Numer. Math., 5 (1997), pp. 211–230.

[60] Ivan Yotov, *Interface solvers and preconditioners of domain decomposition type for multiphase flow in multiblock porous media*, in Scientific computing and applications, vol. 7 of Adv. Comput. Theory Pract., Nova Sci. Publ., Huntington, NY, 2001, pp. 157–167.